

# NAVAL POSTGRADUATE SCHOOL

## Monterey, California



## THESIS

**FINITE ELEMENT MODELING OF METAL FOAM  
STRUCTURES SUBJECT TO COMPRESSIVE LOADING**

by

Rabon E. Cooke

December 2001

Thesis Advisor:

Young W. Kwon

**Approved for public release; distribution is unlimited**

Report Documentation Page		
<b>Report Date</b> 19 Dec 2001	<b>Report Type</b> N/A	<b>Dates Covered (from... to)</b> -
<b>Title and Subtitle</b> Finite Element Modeling of Metal Foam Structures Subject to Compressive Loading	<b>Contract Number</b>	
	<b>Grant Number</b>	
	<b>Program Element Number</b>	
<b>Author(s)</b> Cooke, Rabon E.	<b>Project Number</b>	
	<b>Task Number</b>	
	<b>Work Unit Number</b>	
<b>Performing Organization Name(s) and Address(es)</b> Naval Postgraduate School Monterey, California	<b>Performing Organization Report Number</b>	
<b>Sponsoring/Monitoring Agency Name(s) and Address(es)</b>	<b>Sponsor/Monitor's Acronym(s)</b>	
	<b>Sponsor/Monitor's Report Number(s)</b>	
<b>Distribution/Availability Statement</b> Approved for public release, distribution unlimited		
<b>Supplementary Notes</b>		
<b>Abstract</b>		
<b>Subject Terms</b>		
<b>Report Classification</b> unclassified	<b>Classification of this page</b> unclassified	
<b>Classification of Abstract</b> unclassified	<b>Limitation of Abstract</b> UU	
<b>Number of Pages</b> 82		

THIS PAGE INTENTIONALLY LEFT BLANK

<b>REPORT DOCUMENTATION PAGE</b>			<i>Form Approved OMB No. 0704-0188</i>	
Public reporting burden for this collection of information is estimated to average 1 hour per response, including the time for reviewing instruction, searching existing data sources, gathering and maintaining the data needed, and completing and reviewing the collection of information. Send comments regarding this burden estimate or any other aspect of this collection of information, including suggestions for reducing this burden, to Washington headquarters Services, Directorate for Information Operations and Reports, 1215 Jefferson Davis Highway, Suite 1204, Arlington, VA 22202-4302, and to the Office of Management and Budget, Paperwork Reduction Project (0704-0188) Washington DC 20503.				
<b>1. AGENCY USE ONLY (Leave blank)</b>		<b>2. REPORT DATE</b> December 2001	<b>3. REPORT TYPE AND DATES COVERED</b> Master's Thesis	
<b>4. TITLE AND SUBTITLE:</b> Finite Element Modeling of Metal Foam Structures Subject To Compressive Loading			<b>5. FUNDING NUMBERS</b>	
<b>6. AUTHOR(S)</b> Cooke, Rabon E.				
<b>7. PERFORMING ORGANIZATION NAME(S) AND ADDRESS(ES)</b> Naval Postgraduate School Monterey, CA 93943-5000			<b>8. PERFORMING ORGANIZATION REPORT NUMBER</b>	
<b>9. SPONSORING /MONITORING AGENCY NAME(S) AND ADDRESS(ES)</b> N/A			<b>10. SPONSORING/MONITORING AGENCY REPORT NUMBER</b>	
<b>11. SUPPLEMENTARY NOTES</b> The views expressed in this thesis are those of the author and do not reflect the official policy or position of the Department of Defense or the U.S. Government.				
<b>12a. DISTRIBUTION / AVAILABILITY STATEMENT</b> Approved for public release; distribution is unlimited			<b>12b. DISTRIBUTION CODE</b>	
<b>13. ABSTRACT (maximum 200 words)</b>  <p>A unit-cell model was developed for open metallic foams in order to predict their effective elastic moduli and the plastic collapse strengths. The model is based on the metallic ligament frame of tetrakaidecahedral shape. The frame structure of the unit-cell was analyzed using the finite element method. The plastic collapse strength was determined when the joints of ligaments became plastic hinges under the assumption of elastic-perfectly plastic material behavior of the metallic material. Both elastic modulus and plastic collapse strength were computed using a single step of finite element analysis without any iterative or incremental procedure. In addition, a very small number of finite elements used. As a result, the unit-cell is computationally very efficient. The next study considered the effective elastic moduli and plastic collapse strengths of the same metallic foams filled with a viscoelastic material. For this study, the unit-cell model was modified. The model considered the ligament frame structure supported by viscoelastic foundation that represented the filler material. In order to validate the unit-cell models, experiments were also conducted. The experimental data agreed very well with the predicted values of both stiffness and strength.</p> <p>Proper design of the materials studied here can have high strength and stiffness, low weight, high damping properties so that they may be useful for multifunctional materials that can be used in the Navy and Department of Defense applications.</p>				
<b>14. SUBJECT TERMS</b> aluminum metal foam, composite metal foam, metal foam compressive loading, metal foam stiffness, metal foam strength			<b>15. NUMBER OF PAGES</b> 66	
			<b>16. PRICE CODE</b>	
<b>17. SECURITY CLASSIFICATION OF REPORT</b> Unclassified	<b>18. SECURITY CLASSIFICATION OF THIS PAGE</b> Unclassified	<b>19. SECURITY CLASSIFICATION OF ABSTRACT</b> Unclassified	<b>20. LIMITATION OF ABSTRACT</b> UL	

THIS PAGE INTENTIONALLY LEFT BLANK

Approved for public release; distribution is unlimited

**FINITE ELEMENT MODELING OF METAL FOAM STRUCTURES SUBJECT  
TO COMPRESSIVE LOADING**

Rabon E. Cooke  
Lieutenant Commander, United States Navy  
B.S., United States Naval Academy, 1987

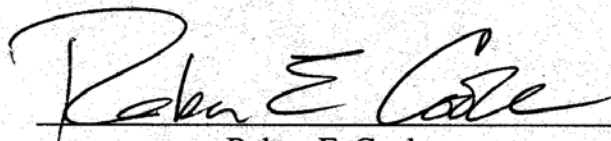
Submitted in partial fulfillment of the  
requirements for the degree of

**MASTER OF SCIENCE IN MECHANICAL ENGINEERING**

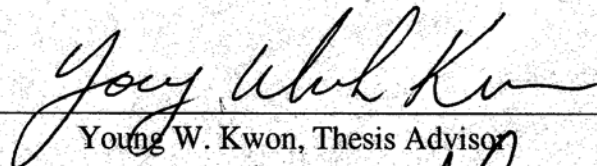
from the

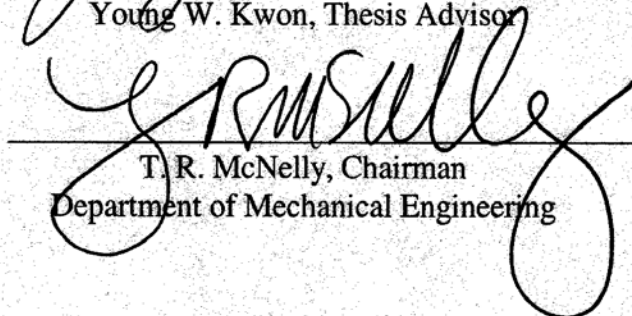
**NAVAL POSTGRADUATE SCHOOL  
December 2001**

Author:

  
Rabon E. Cooke

Approved by:

  
Young W. Kwon, Thesis Advisor

  
T. R. McNelly, Chairman  
Department of Mechanical Engineering

THIS PAGE INTENTIONALLY LEFT BLANK

## **ABSTRACT**

A unit-cell model was developed for open metallic foams in order to predict their effective elastic moduli and the plastic collapse strengths. The model is based on the metallic ligament frame of tetrakaidecahedral shape. The frame structure of the unit-cell was analyzed using the finite element method. The plastic collapse strength was determined when the joints of ligaments became plastic hinges under the assumption of elastic-perfectly plastic material behavior of the metallic material. Both elastic modulus and plastic collapse strength were computed using a single step of finite element analysis without any iterative or incremental procedure. In addition, a very small number of finite elements used. As a result, the unit-cell is computationally very efficient. The next study considered the effective elastic moduli and plastic collapse strengths of the same metallic foams filled with a viscoelastic material. For this study, the unit-cell model was modified. The model considered the ligament frame structure supported by viscoelastic foundation that represented the filler material. In order to validate the unit-cell models, experiments were also conducted. The experimental data agreed very well with the predicted values of both stiffness and strength.

Proper design of the materials studied here can have high strength and stiffness, low weight, high damping properties so that they may be useful for multifunctional materials that can be used in the Navy and Department of Defense applications.



THIS PAGE INTENTIONALLY LEFT BLANK

# TABLE OF CONTENTS

<b>I.</b>	<b>INTRODUCTION.....</b>	<b>1</b>
<b>II.</b>	<b>BACKGROUND.....</b>	<b>3</b>
<b>A.</b>	<b>LITERATURE SEARCH.....</b>	<b>3</b>
<b>B.</b>	<b>SPACE FILLING STRUCTURES.....</b>	<b>4</b>
<b>1.</b>	<b>CUBIC STRUCTURE .....</b>	<b>7</b>
<b>2.</b>	<b>TETRAKAIDECAHEDRON.....</b>	<b>9</b>
<b>3.</b>	<b>WEAIRE-PHELAN UNIT CELL .....</b>	<b>10</b>
<b>C.</b>	<b>THEORIES.....</b>	<b>12</b>
<b>1.</b>	<b>Elastic Failure versus Plastic Collapse.....</b>	<b>12</b>
<b>2.</b>	<b>Gibson and Ashby Cell Theory.....</b>	<b>13</b>
<b>a.</b>	<b><i>Open Cell Theory</i>.....</b>	<b>13</b>
<b>b.</b>	<b><i>Closed Cell Theory</i> .....</b>	<b>14</b>
<b>2.</b>	<b>Euler-Bernoulli Frame Structure .....</b>	<b>15</b>
<b>3.</b>	<b>Beams and Frames on Elastic Foundation.....</b>	<b>15</b>
<b>III.</b>	<b>FINITE ELEMENT MODEL.....</b>	<b>17</b>
<b>A.</b>	<b>UNIT CELL MODEL WITHOUT FILL MATERIAL.....</b>	<b>18</b>
<b>1.</b>	<b>Model Description .....</b>	<b>18</b>
<b>2.</b>	<b>Model Material Properties .....</b>	<b>20</b>
<b>B.</b>	<b>UNIT CELL MODEL WITH FILL .....</b>	<b>21</b>
<b>1.</b>	<b>Model Description .....</b>	<b>21</b>
<b>3.</b>	<b>Model Material Properties .....</b>	<b>21</b>
<b>IV.</b>	<b>EXPERIMENTS.....</b>	<b>23</b>
<b>A.</b>	<b>OPEN CELL ALUMINUM METAL FOAM.....</b>	<b>23</b>
<b>B.</b>	<b>ALUMINUM METAL FOAM FILLED WITH ELASTO-PLASTIC MATERIAL.....</b>	<b>24</b>
<b>V.</b>	<b>DISCUSSION AND RESULTS .....</b>	<b>27</b>
<b>A.</b>	<b>OPEN CELL ALUMINUM METAL FOAM.....</b>	<b>27</b>
<b>B.</b>	<b>FILLED ALUMINUM FOAM .....</b>	<b>39</b>
<b>VI.</b>	<b>CONCLUSION AND RECOMMENDATIONS .....</b>	<b>43</b>
<b>APPENDIX A:</b>	<b>STIFFNESS AND MASS MATRICES .....</b>	<b>45</b>
<b>APPENDIX B:</b>	<b>STRESS-STRAIN DIAGRAMS .....</b>	<b>51</b>
<b>1.</b>	<b>10 PPI .....</b>	<b>51</b>
<b>2.</b>	<b>20 PPI .....</b>	<b>52</b>

3.	40 PPI .....	53
4.	10 PPI + FILL MATERIAL .....	54
5.	40 PPI + FILL MATERIAL .....	55
APPENDIX C: SCANNING ELECTRON MICROSCOPE IMAGES .....		57
1.	10 PPI IMAGES .....	57
2.	20 PPI IMAGES .....	59
3.	40 PPI IMAGE .....	61
LIST OF REFERENCES .....		63
INITIAL DISTRIBUTION LIST .....		65

## LIST OF FIGURES

Figure 1	Cubic Cell.....	7
Figure 2	Tetrakaidecahedron .....	9
Figure 3	Weaire – Phelan Cell .....	11
Figure 4	10 PPI Stress vs. Strain (Expanded).....	23
Figure 5	10 PPI Stress vs. Strain .....	24
Figure 6	10 PPI with Elasto-plastic Fill Material (Expanded) .....	25
Figure 7	10 PPI with Elasto-Plastic Fill Material.....	25
Figure 8	10 PPI Aluminum Compressed Cell .....	29
Figure 9	20 PPI Aluminum Compressed Cell .....	30
Figure 10	40 PPI Aluminum Compressed Cell .....	31
Figure 11	Relative Stiffness vs. Relative Density .....	32
Figure 12	Relative Strength vs. Relative Density.....	33
Figure 13	SEM Image of 10 PPI Aluminum Foam Before Compression .....	35
Figure 14	SEM Image of 10 PPI Aluminum Foam After Compression.....	36
Figure 15	Filled Metal Foam Relative Stiffness vs. Relative Density .....	39
Figure 16	Filled Metal Foam Relative Strength vs. Relative Density .....	40
Figure 17	10 PPI Stress vs. Strain (Expanded).....	51
Figure 18	10 PPI Stress vs. Strain .....	51
Figure 19	20 PPI Stress vs. Strain (Expanded).....	52
Figure 20	20 PPI Stress vs. Strain .....	52
Figure 21	40 PPI Stress vs. Strain (Expanded).....	53
Figure 22	40 PPI Stress vs. Strain .....	53
Figure 23	10 PPI + Fill Stress vs. Strain (Expanded).....	54
Figure 24	10 PPI + Fill Stress vs. Strain.....	54
Figure 25	40 PPI + Fill Stress vs. Strain (Expanded).....	55
Figure 26	40 PPI + Fill Stress vs. Strain.....	55
Figure 27	SEM Image of 10 PPI Aluminum Foam Before Compression .....	57
Figure 28	SEM Image of 10 PPI Aluminum Foam After Compression.....	58
Figure 29	SEM Image of 20 PPI Aluminum Foam Before Compression .....	59
Figure 30	SEM Image of 20 PPI Aluminum Foam After Compression.....	60
Figure 31	SEM Image of 40 PPI Aluminum Foam Before Compression .....	61
Figure 32	SEM Image of 40 PPI Aluminum Foam After Compression.....	62

THIS PAGE INTENTIONALLY LEFT BLANK

## LIST OF TABLES

Table 1	Cell Geometry .....	8
Table 2	Bulk Aluminum Material Properties .....	20
Table 3	Fill Material Properties.....	21
Table 4	Change in Maximum Displacement and Moment vs. Number of Finite Elements .....	28
Table 5	Beam Theory And Finite Element Model Predicted Natural Frequency .....	37
Table 6	Predicted Strength In Open Cell versus Filled Cell .....	41
Table 7	Predicted versus Observed Yield Strength.....	42

THIS PAGE INTENTIONALLY LEFT BLANK

## **ACKNOWLEDGMENTS**

The author wishes to acknowledge his thesis advisor, Dr. Young Kwon, for his assistance, guidance and patience. Without his guidance and wisdom this project would not have been a success.

The author wishes to acknowledge Dr. Chanman Park for his assistance in sample preparation, testing and expertise in metal foam construction.



THIS PAGE INTENTIONALLY LEFT BLANK

## I. INTRODUCTION

The cell represents a finite partition in space and volume and is typically considered the fundamental unit or division of a structure. Cellular materials are abundant in nature. They are as diverse as the basic building block of a bees hive, to the fine structure of an insect's wing, to the complex structure of human bone. The most common structure composed of a cellulous form is wood. This framework has also been copied to form modern building materials from liquid metals to plastic composites. Metals and plastics that are formed to produce a continuous cellular structure are often referred to as foams.

The maritime and aerospace industries use metal and composite foam materials for their strength and insulative properties. The foam materials provide a means to obtain good strength properties with a significant reduction in material weight. Additionally, the use of foams made from viscoelastic material has the potential for applications in vibrations and acoustic systems.

Analysis of foam materials requires an understanding of the relationship between the cellular structure and the density of the base material from which that structure is formed. It can be shown that as the basic cell becomes denser it would develop properties very similar to a solid entity of the original material. However as the base material becomes more porous the mechanism for determining strength are varied depending on such factors as cell geometry and method of loading. The analysis of these factors is very important if foam materials will be used in structural applications.

The analysis of the failure location and mechanism of cell structures has been undertaken primarily from experimental and empirical methods. The relationship between the base material density and the average cell density is used to determine empirical formulae, which allows some useful prediction of average strength. These analyses do not attempt to characterize the size or shape of any cell, but instead assume a uniform random dispersion throughout any matrix of interest. The use of the empirical equation approach has proven to be satisfactory for various applications. However, if more precise results are required, then additional experimental analysis was required to

determine specific material properties. Similarly, very little empirical data has been accumulated on the vibration associated with foam materials. This again requires experimentation if material vibratory response is necessary information.

Our research has taken the approach that the strength, stiffness and dynamic characteristics such as natural frequency can be determined using a repetitive unit cell structure, which is not truly random, but would accurately represent a typical cross section of a foam material. This cell chosen would accurately reflect possible modes of failure and would allow a more precise understanding of failure locations and value without having to conduct multiple experiments. The model will be correlated with empirical study models and validated against experimental results. The deformation and mode of failure will be confirmed using results obtained from scanning electron microscope (SEM) analysis of the representative foam materials

## **II. BACKGROUND**

### **A. LITERATURE SEARCH**

The characterization of metal foam structures first required an understanding of basic geometric structures and systems. Gibson and other researchers [1-3] have shown that the organization of a foam material is a repeating matrix geometry. If the geometry can be identified mathematically, then an analytical model could be developed which represents the behavior of a cell like structure. Classical geometry has been studied throughout the ages. Great philosophers and mathematicians, such as Plato and Archimedes, first proposed the basic polyhedrons that may be used to represent a cell. The regular structures proposed by Plato and the semi-regular structures of Archimedes represent the fundamental building solutions from which almost all uniform repeating structures in nature are formed. Although cells in nature are not the perfect regular structures proposed by Plato and Archimedes, it is possible to use these shapes to represent the cellular matrix of foam.

Multiple texts [4,5] are available to help explain the angular and spatial relationship between various elements of the unit cell. The classic cube is easiest to visualize. However, as the geometry becomes more complex, it is increasingly difficult to observe the mathematical relationships. Beyond the basic angular relationships it is necessary to determine which structural geometry will accurately represent any matrix. Lord Kelvin in 1887 [2] proposed geometry for soap bubble formation that represented the physical relationship.

The analysis of a three-dimensional repeating foam matrix is very similar to that of the repeating lattice space structure. Numerous methods have been proposed for the analysis of truss and lattice structures. One such method review was the continuum model proposed by Noor, Anderson and Greene [6]. Their approach is advantageous in that it allows a practical solution method for overall response and is particularly useful from the preliminary design point of view. The continuum model presented was useful

for large lattice structures where a very limited number of finite elements are used to produce an analytic solution.

Noor [3] proposed a second continuum model approach for analysis of space structures. This model was particularly useful for determining the global spectral response of rigid jointed lattice structures. This approach was advantageous in allowing local member deformations to be neglected provided these deformations within the motions of interest were small.

Gibson and Ashby [1] proposed a theoretical approach for determining the strength and other material characteristics of foam structures. This comprehensive work is the basis for the theoretical relationship between a homogenous solid and a porous cell with equivalent base materials. From this work the basic cell relationship for stiffness and strength are empirically derived.

Roberts and Garboczi [7] investigated the random nature of cellular solids and used a finite element method to compute the microstructure dependence of the Young's Modulus and Poisson's ratio. They found that the theoretical relationship between density and Young's Modulus is more complex than the commonly referenced empirical relationship of the Gibson and Ashby [1] model. Additionally it was noted that for certain geometries under uniform axial compression, the forces are balanced so the central node is locked in position. This results in deformations only along the axial directions of any strut.

## **B. SPACE FILLING STRUCTURES**

The analysis of foam materials begins with an understanding of the structures required to develop a physical model of the space enclosed. The cell is the basic building block for analysis. The cell can be decomposed into three components, these being vertices (V) (or nodes), which are joined by edges (E), which then surround faces (F). Plato and Archimedes first proposed a concept of basic polyhedrons formed from a combination of edges and faces. Plato [8] showed that there exist only five regular

polyhedrons. These are limited to the cube, dodecahedron, tetrahedron, icosahedron, and the octahedron. These polygons are referred to as regular because all edge lengths are equal in every face. Archimedes [9] contributed to the general body of knowledge by combining the basic regular polyhedron to form a series of semi-regular polyhedrons. Archimedes showed that there exist only thirteen possible semi-regular polyhedrons. The semi-regular polyhedra faces are composed of only regular planar geometries that repeat in a predictable manner.

The study of geometry in three-dimensional cellular solids is very applicable to foam analysis. Although foams do not appear as a completely uniform structure in nature, they do follow basic topographical relations. Euler [4], in 1746, proposed a mathematical relation among the edges (E), faces (F), and vertices (V), which compose given cell (C).

$$-C + F - E + V = 1 \quad (1)$$

Using the Euler mathematical model, a set ratio among the faces, edges and vertices allow the angle of incidence between any two planes to be determined. Knowledge of the internal angles then defines the volume enclosed within the solid.

In nature area and volume are conserved. This requires that for any pure geometry to fill space when stacked together the faces of one cell must uniformly intersect with those adjoining and when completely surrounded, there is no void. The polyhedra, which are capable of repeated joining in a void free condition, are referred to as space filling. Of the Platonic and Archimedic solids only the cube and the tetrakaidecahedron (truncated octahedron) are space filling. Lord Kelvin [2], in 1887, showed that the space-filling regular polyhedron, which minimizes surface area per unit volume, was the tetrakaidecahedron. It took over one hundred years, using modern computer optimization methods, for Weaire and Phelan (1994) to develop a unit structure which had a lower surface area to volume ratio.

Each of the space filling polyhedron has been used at some point to define cell foam structures. A brief description of the cube, tetrakaidecahedron and Weaire/Phelan ball are provided.

THIS PAGE INTENTIONALLY LEFT BLANK

## 1. CUBIC STRUCTURE

The cube cell is composed of six square faces, eight vertices and twelve edges. As previously noted, this structure is the only regular polyhedron that fills space. Table 1 summarizes the principal properties. The cubic structure has been used extensively to develop the analytic relations between the geometry and material properties. The relatively simple formulation of the cube is both its advantage and disadvantage. Although it is very easy to visualize, it does not accurately represent the space filling characters of bubbles within a metal foam material.

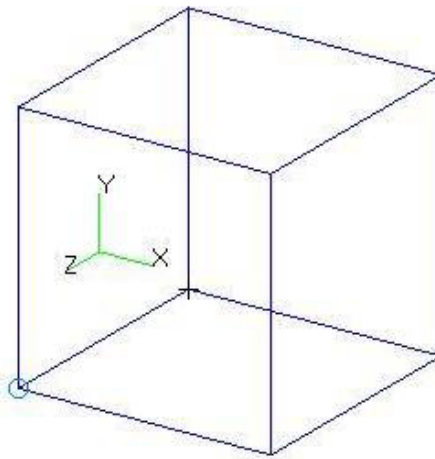


Figure 1 Cubic Cell

When calculating the properties of a cell, an important consideration is the relative size between the edge length, edge thickness and whether the faces are considered open or closed. A closed face cell will not allow free transport of a fluid between adjacent cell chambers. Open cell foam may be thought of as wire frame cells where the edges occupy a finite volume. Any fluid contained within the enclosed volume of an open cell structure is allowed to freely transport between successive cells. This property of open or closed cell structure is made extensive use in commercial applications. Personal floatation devices for water activities are examples of where closed cell foams are used. The air contained within the cell pockets provides the added



buoyancy because it is not allowed to escape. For open cell foams, as the volume of the edges increase, the potential exists for the condition that the space between edges restricts the flow of volume between adjacent cells. This effect is more pronounced as the fluid within the cell membrane becomes more viscous. The restriction of flow may act as a constraining force on the cell edges when loads are applied.

The face of closed cell foams will behave similar to a thin shell subjected to the combined loading of face pressure, edge loading and edge shear. These factors may be significant in determining the structural properties of the cell. Similarly, open cell foam will exhibit different properties depending upon the relative volume of the edges compared to the overall volume of the cell. If the cross sectional area of the edge is small relative to the edge length, then when subjected to compressive axial loading buckling may be of major concern.

The cubic models simplicity may be adequate when considering only simple axial compression or tension. However, Gibson and Ashby [1] and Roberts and Garboczi [7] noted that the model would not accurately predict distortion due to out of plane loading. Similarly, if loading along the structure is not at a vertex the model has difficulty accounting for the bending loads and distortions. This resulting anisotropy therefore makes the cube a less desirable model solution.

Cell Geometry	Number of Faces	Number of Edges	Number of Vertices	Cell Surface Area*	Cell Volume*
Cube	6	8	12	6	1
Tetrakaidecahedron	14	36	24	26.80	11.31
Weaire-Phelan	14	24	12	26.71	11.31
*area and volume areas are based on a unit vertex length					

Table 1 Cell Geometry

## 2. TETRAKAIDECAHEDRON

A more complex and accurate approach to modeling bubble formation within foam was taken by Lord Kelvin in 1887. Kelvin was searching for the most efficient manor to fill space within a given volume. Kelvin looked for a repeating structure that would provide the minimum surface area per a given volume. The most efficient shape he devised was the tetrakaidecahedron or regular truncated octahedron. Eight regular hexagons and six squares make up the fourteen faces that characterize the tetrakaidecahedron. Thirty-six (36) edges and twenty-four (24) vertices connect the faces. The volume and area properties are summarized in Table 1. Figure 2 shows a representation of the truncated octahedron. The beauty in the Kelvin's pattern is the repeatability of the matrix within any structure.

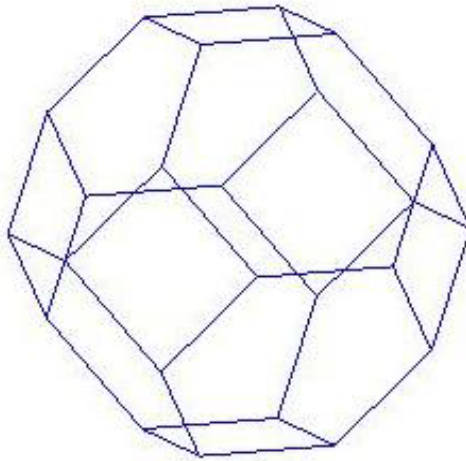


Figure 2 Tetrakaidecahedron

Other researchers have recently explored the tetrakaidecahedron as a means for modeling foam structures. Zhu, Mills and Knott [10] theorized that this model lattice would display isotropic properties throughout the elastic region. Their theoretical analysis showed good correlation with real materials in most cases. Significant variation in Young's Modulus between the theoretical and observed values was noted at increasing ratio of foam to solid density. This was an area requiring greater study and analysis.

The tetrakaidecahedron model appears very consistent with many foam and bubble formations observed in nature. The relative ease for which this model is constructed and its potential for accurate prediction of real solid behavior make it a prime candidate for further study.

### **3. WEAIRE-PHELAN UNIT CELL**

It has taken over 100 years to find another cell structure that is more efficient at filling space than the Kelvin ball. Weaire and Phelan [11] reported in 1994 that a more efficient structure could be developed. Their approach was to use computer optimization methods to sequentially reduce the surface area. The Weaire-Phelan structure is composed of six tetrakaidecahedra and two dodecahedra arranged to display fourteen faces with twenty-eight edges and twelve vertices. This arrangement results in a 0.3% reduction in the overall surface area. Figure 3 is a picture of this structure. There is no mathematical proof that this structure is the optimal space filling structure.

The structure of the Weaire-Phelan cell should permit the modeling of real foams with very limited anisotropy. The very few parallel faces will allow limited distortion effects.

This model has recently developed more interest as a potential pattern for foam analysis. Although it is slightly more space filling than the Kelvin ball, the relative difficulty to develop a mathematical model limits its use. Additionally, the random nature of bubbles and foam cell structures does not indicate that there is significant benefit to be gained from the slight reduction in surface area.

Bubble formation within a cell is never purely regular. Therefore, the use of either the Weaire – Phelan or Kelvin model will not accurately represent a real foam solid under all conditions. Although efficient space filling is an important criterion for modeling the foam, other influences must be considered. Surface tension between adjoining cells will contribute to some rotation within the edges to achieve the optimum

intersection between vertices. Another impact on the foam model is the volume fraction of solid present in the edges and face structures. Surface tension will tend to draw more mass towards the edges and this is then more heavily weighted towards the vertices. Any model developed must balance the impact of these competing influences.

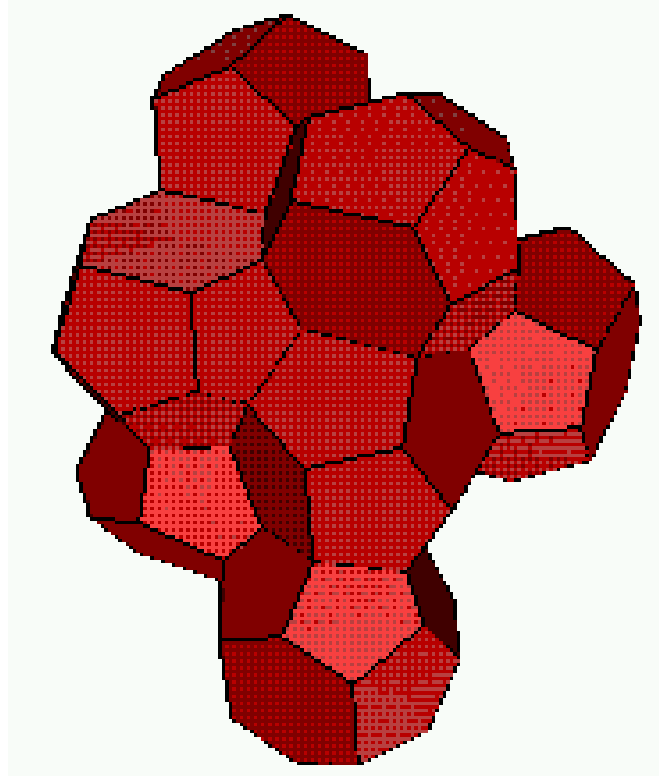


Figure 3 Weaire – Phelan Cell (From: Foam Physics Group, TCD [12])

## C. THEORIES

### 1. Elastic Failure versus Plastic Collapse

The mechanism of failure for cell edges under compressive load will dependent upon the slenderness ratio of the cell edge. For the cell geometries of interest, the edges are first observed to bend and then buckle. Elastic Failure i.e. buckling will occur if the axial load in an edge exceeds a critical value. The failure load for a slender beam with simple supports is determined using Euler's formula and is

$$F_{crit} = \frac{n^2 \pi^2 EI}{l^2}. \quad (2)$$

where  $n$ , is the modal number and is proportional to the number of restraints in the system and is an integer value. The lowest critical load occurs for the mode of  $n = 1$ . This is the critical mode, which was used for analysis of the tetrakaidecahedron.  $l$  is the effective length of the beam depending on the boundary conditions.

A beam subjected to a bending moment will experience tension or compression depending on the location relative to the neutral axis. The fully plastic moment occurs when all fibers within the beam experience yielding by either tension or compression. At this point the beam is said to have reached plastic collapse. Hodge [13] tabulates the fully plastic moment for common beam sections. A rod of uniform circular cross-section was assumed for analysis in this study. The fully plastic moment is  $M = \frac{4}{3} \sigma_o R^3$  where  $R$  is the rod radius and  $\sigma_o$  is the yield stress with perfectly plastic deformation.

## 2. Gibson and Ashby Cell Theory

### a. Open Cell Theory

Ko [14] first developed the relation between density and Young's Modulus for a cubic unit cell. Gibson and Ashby [1] further refined and generalized the analysis and developed the basic equations that form the analytic solution for foams.

The solid fraction for open cell foam is generally accepted as  $\frac{\rho^*}{\rho_s} \approx \left(\frac{t}{l}\right)^2$

where,  $t$  is the thickness of a cell edge and  $l$  is the length of the cell edge. Young's Modulus for the foam is then calculated as  $\frac{E^*}{E_s} = C \left(\frac{\rho^*}{\rho_s}\right)^2$ , where  $C$  is a proportionality constant accounting for the variation in cell structure. This result has been confirmed through experimental observation.

The strength of the structure is then dependent upon the ratio of the edge thickness to length. Gibson and Ashby [1] address two possible failure mechanisms for the foam cell, one mechanism is reaching the elastic limit, and the second is plastic failure. Failure by either mechanism is possible and is dependent upon the relative ratio between the cell length and thickness and the elastomeric properties of the solid metal. The elastic collapse of a structure occurs when the applied load exceeds the critical load for buckling. The plastic collapse of an edge structure occurs when the fully plastic moment is exceeded. For relatively slender cell edges, under compressive load, it is possible for the elastic limit to be exceeded prior to the plastic collapse.

Gibson and Ashby [1] determined, through experimental observation, the following empirical relations for open cell foams.

$$\sigma_{el}^* \approx E_s^* 0.03 \left(\frac{\rho^*}{\rho_s}\right)^2 \left(1 + \left(\frac{\rho^*}{\rho_s}\right)^{1/2}\right)^2 \quad (\text{for elastic limit}) \quad (3)$$

$$\sigma_{pl}^* \approx \sigma_{ys}^* 0.23 \left( \frac{\rho^*}{\rho_s} \right)^{3/2} \left( 1 + \left( \frac{\rho^*}{\rho_s} \right)^{1/2} \right) \quad (\text{for plastic failure}) \quad (4)$$

### ***b. Closed Cell Theory***

Gibson and Ashby [1] developed similar relation for the closed cell condition. The closed cell case must account for the added rigidity of the cell provided by the face structure. This added stiffness results in less total cellular distortion. A significant difference between the open cell and closed cell is that relative density shows a more linear relation with the edge thickness to length ratio i.e.  $\frac{\rho^*}{\rho_s} \approx \left( \frac{t}{l} \right)$ . This linear relation is evident in the analytic solutions developed for the elastic and plastic collapse strengths.

The closed cell analytic solution assumes that the rigid wall structure provides support to the edges and increases overall cell stiffness. This solution approach may be applicable for analyzing open cell foams that are immersed or encased in a very viscous fluid. The dense cell fluid will provide added stiffness to the cell edges, which will manifest properties of a more rigid structure, like closed cell foam. Similarly, if the internal volume of the cell is built of an elastomeric material then the closed cell formulation may also provide a first analysis for strength. A closed cell analysis could assume that the wall material will have the same stiffness properties as the edge elements. Although this is not completely accurate, a first approximation is achievable which may be valuable. A more refined approach would be to provide a composite value for stiffness of the cell based on the base cell properties and those of the elastomeric material. The difficulty with this approach will be properly proportioning the stiffness between the base and fill material.

## 2. Euler-Bernoulli Frame Structure

The cell may be considered as a frame structure with the vertices acting as clamped end joints. Euler-Bernoulli [16] beam bending is then applied to the edge elements to analyze the cell properties. The general Euler-Bernoulli [16] equation for beam bending is

$$\bar{\rho} \frac{\partial^2 v}{\partial t^2} + \frac{\partial}{\partial x^2} \left( EI \frac{\partial^2 v}{\partial x^2} \right) = P(x, t). \quad (5)$$

The  $x$  direction within the beam is defined along the axis between the two clamped ends. Solving the differential equation we find  $v(x, t)$ , the displacement perpendicular to the rod axis as a function of both the distance along the rod,  $x$  and time,  $t$ . Note that in the differential equation,  $v(x, t)$  is also a function of the mass per unit volume  $\bar{\rho}$ , the beam rigidity  $EI$ , and the applied pressure loading  $P(x, t)$ .

The edges of the cell are considered uniform rods with constant cross-sectional area and uniform density. In bubbles formed within foam, surface tension effects cause a disproportionate distribution of element volume at the vertices. This mass distribution will impact the inertial and strength properties of the rod. This affect has been studied by Mills [15] and can be assumed negligible for global analysis of foam behavior.

The Euler-Bernoulli beam bending equation must be expanded for our cell to account for the axial deformation, rotation along the rod and shear deformation in three dimensions. For our analysis we neglect the coupling between the deformations and assume all displacements are small.

## 3. Beams and Frames on Elastic Foundation

When open cell foams are filled with an elastomeric material their strength properties are not well modeled by either the open or closed cell analytic model. The fill material will provide some additional rigidity to the matrix. The composite material will assume a combination of mechanical properties that are similar to both the elastomeric material and the foam shell. The Winker model [13] provides a method to account for the stiffness of the fill material and its influence on the cell edge. The Winkler model



assumes the beam is supported on an elastic foundation that produces a linear proportional reaction force  $R$  with respect to the deflection of the beam  $v$ . The constant of proportionality relating force and displacement is  $k$  and this is related to the stiffness of the foundation material. Ugural and Fenster [16] provide a general approach to develop an equation of similar form to the Euler-Bernoulli equation. This relation is illustrated below.

$$\bar{\rho} \frac{\partial^2 v}{\partial t^2} + \frac{\partial}{\partial x^2} \left( EI \frac{\partial^2 v}{\partial x^2} \right) + kv = P(x, t) \quad (6)$$

Note the stiffness relation  $EI$  in this equation refers to the beam and the stiffness properties of the foundation are contained within the constant  $k$ . The elastic foundation constant  $k$  is computed from:

$$k = \frac{8\pi G(1-\nu)}{(3-4\nu)K_0(2\pi r/\delta) + (\pi/\delta)K_1(2\pi r/\delta)} \quad (7)$$

where  $G$  is the shear modulus of the filler,  $\nu$  is Poisson's ratio of the filler,  $r$  is the radius of the ligament,  $\delta$  is the ligament length and  $K_0$ ,  $K_1$  are the zeroth order and first order modified Bessel function of the second kind, respectively.

### III. FINITE ELEMENT MODEL

The goal of finite element modeling is to develop a simple model, which accurately represents the behavior of real structures, subjected to compressive loading. The model must accurately predict when plastic collapse will occur within the cell. The modeling method chosen was similar to that developed by Kwon and Bang [17]. Mills [15] discussed the possibility for improper strength and stiffness determination when an over simplified model of the foam cell was used to predict real foam behavior. Consider the case of the simple cubic geometry. When the cell is uniformly load on a face, such that the load application points are at the vertices, there is no bending moment induced in the edges. This results in a very high strength and stiffness. However if the same load is applied at the center of each edge, a significant bending moment is created. The difference in cell behavior, depending on the application of loading is referred to as anisotropic behavior [1,21]. Anisotropic behavior is not a desirable characteristic for a unit cell.

The tetrakaidecahedron structure was chosen as the basic cell unit for analysis. The finite elements were developed using Galerkin's method and linear shape functions for a rod of uniform geometry and material properties. Each node of the rod element was allowed a total of six degrees of freedom, three in translation and three rotation. The model assumes linear elastic behavior throughout all motions.

Compressive behavior for the cell was modeled as uniform point loads attached to the square face nodes associated with the unit cell. The advantage of the tetrakaidecahedral structure is, when loaded at the vertices or along any point of the face, no edge is in direct axial loading. Ensuring that no direct axial loading occurs on any edge eliminates the potential for anisotropic behavior to be displayed from the model.

The mathematical computing language MATLAB was used to for the finite element programming. An *Excel* spreadsheet was used to post-process the MATLAB results and to compute cell stiffness and strength.

## A. UNIT CELL MODEL WITHOUT FILL MATERIAL

### 1. Model Description

The repeating geometry of the tetrakaidecahedron is the basis for the finite element model. All edges of the cell were assumed uniform rods. The finite element method allows each edge element to be discretised as a finite number of uniform rods, which are coupled at the nodes. Kwon and Bang [17] developed Hermitian shape functions for the three-dimensional frame structure. These shape functions were used to compute the element stiffness matrix.

The displacement of the finite element is calculated from the known forces applied to the body and the stiffness properties of each edge element. This basic formulation is written in matrix form as  $[K]\{d\} = \{F\}$ . Where  $[K]$  is the element stiffness matrix,  $\{d\}$  is the nodal displacements and  $\{F\}$  is the applied force.

For a three-dimensional frame structure the stiffness matrix is

$$[K^e] = \begin{bmatrix} K_{11}^e & K_{12}^e \\ K_{21}^e & K_{22}^e \end{bmatrix}. \quad (8)$$

The complete formulation for the stiffness matrix is included in Appendix A.

The individual rod element stiffness matrix is defined in terms of the local coordinate system. The transformation matrix  $[T]$  is used to convert the local stiffness matrix to the global system for which the cell is based. The matrix  $[T]$  is based on the directional cosine values of the rod element relative to the global coordinate system. A complete description of the transformation matrix is included in Appendix A. The effective stiffness matrix for a three-dimensional frame structure is then computed as

$$[\bar{K}^e] = [T]^T [K^e] [T]. \quad (9)$$

The nodal displacements can be determined by solving the matrix equation. The nodal displacements are used to compute strains and stresses within the element.

The dimensions of a unit cell are determined from the known density of the foam. The model mesh allows each cell edge to be segmented into a finite number of rod

elements determined by the user. The length of each rod element is a function of the total number of elements for a particular analysis. The mass of each element is determined as a fraction of the total mass of the cell.

The undamped natural frequency for the structure is determined by using a consistent, or lumped mass matrix. The consistent mass matrix is formulated based on the Hermitian shape function and the density of the rod material. For the consistent mass model a uniform circular rod with mass evenly distributed along the length is assumed. Kwon and Bang [17] developed the consistent mass matrix as follows

$$[M^e] = \int_0^l [H]^T \rho A [H] dx \quad (10)$$

Where  $\rho$  is the mass per unit volume and  $A$  is the rod cross sectional area. The complete matrix is in Appendix A.

The lumped mass model assumes an equal distribution of the mass at the nodal points. This matrix is diagonal with values at the translation degrees of freedom points. An example of the lumped mass matrix is included in Appendix A. Similar to the stiffness matrix, the mass matrix must also be transformed to the global axis system. This transformation is

$$[\bar{M}^e] = [T]^T [M^e] [T]. \quad (11)$$

The natural frequency of the global structure is determined based on the free vibration analysis as shown by Kwon and Bang [17].

$$([K] - \omega^2 [M]) \{\bar{d}\} = 0 \quad (12)$$

where  $\omega$  is the angular natural frequency in radians and  $\{\bar{d}\}$  is the mode shape. The mode shape is an eigenvector and is based on the cell response.

Exploiting the symmetry observed in the tetrakaidecahedron structure reduces the computational complexity of the model. This allows using only one eighth of the model structure for calculation.

## 2. Model Material Properties

The material properties of 6061 Aluminum were used for the analysis. This material was chosen to support supplemental experimentation. Table 2 summarizes the material properties of the bulk solid. The density of the foam varies with the average pore size within the foam. This density is determined from initial volume and mass measurements.

Aluminum	
Density	2.70 g/cc
Yield Strength	240 MPa
Young's Modulus	70 GPa
Poisson ratio	0.3

Table 2 Bulk Aluminum Material Properties

## B. UNIT CELL MODEL WITH FILL

### 1. Model Description

The formulation for the basic tetrakaidecahedron model was the same between the filled and unfilled condition. The model exception occurs in determination of the element stiffness matrix. The filler material is modeled as the elastic foundation for the element rods. The effective stiffness matrix is modified for the elastic foundation by adding in the rigidity properties of the fill material. Therefore,

$$\left[ \bar{K}^e \right]_{Filled} = \left[ K^e \right]_{Unfilled} + \left[ K^e \right]_{Foundation} \quad (13)$$

The complete matrix for the fill material  $[K_f^e]$  is included in Appendix A.

### 3. Model Material Properties

Base material properties for the edge elements are unchanged. Filler material properties are given below in Table 3.

Elasto-Plastic Fill	
Density	0.94 g/cc
Young's Modulus	54 MPa
Shear Modulus	5.1 MPa
Poisson ratio	0.4

Table 3 Fill Material Properties

THIS PAGE INTENTIONALLY LEFT BLANK

## IV. EXPERIMENTS

### A. OPEN CELL ALUMINUM METAL FOAM

Model testing on open cell model foam was conducted on three different foam specimens ranging in relative pore density from 10 to 40 pores per inch. The foam was cut into rectangular shape segments with a compressive load applied to the edges. The displacement of the foam was measured to compare with analytic models. Stress-strain diagrams were developed to determine the modulus through the linear elastic region. Figure 4 and Figure 5 show typical experimental results. Stresses vs. strain plots are included in Appendix B for other foam density experiments. This data compares favorably with that expected from the theoretical approximations.

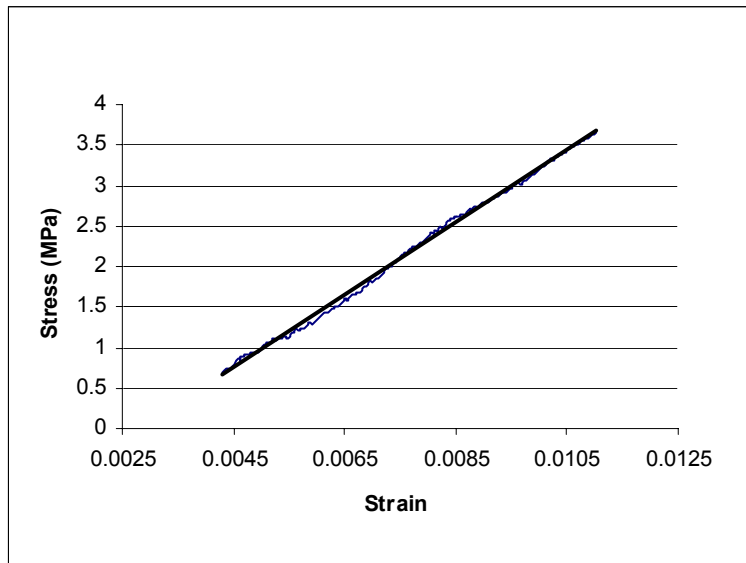


Figure 4 10 PPI Stress vs. Strain (Expanded)



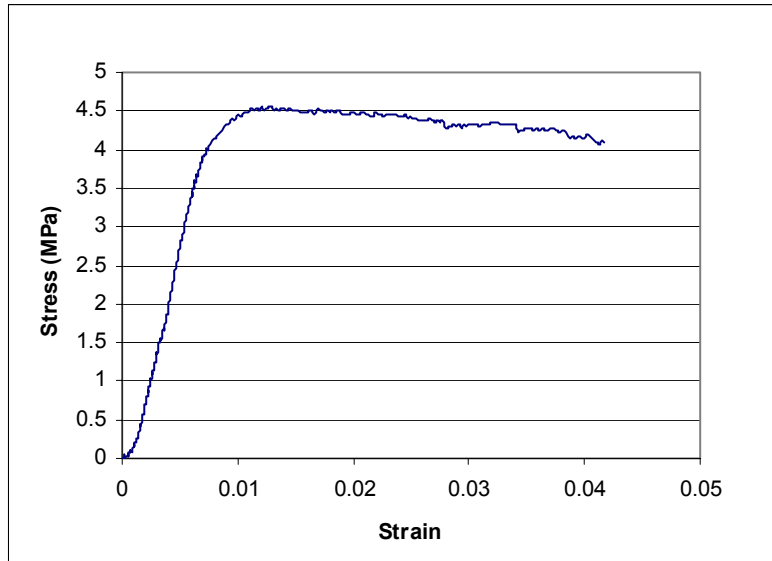


Figure 5 10 PPI Stress vs. Strain

## **B. ALUMINUM METAL FOAM FILLED WITH ELASTO-PLASTIC MATERIAL**

The filled foam structure was constructed by injecting a liquid elasto-plastic material into the pores. The filler material was then allowed to solidify until no liquid was present. The filled foam, materials were then subjected to compressive loading. The results were analyzed to compare with predicted stress versus strain behavior. Figure 6 and Figure 7 show the resulting stress-strain curve in the psuedo-linear elastic region.

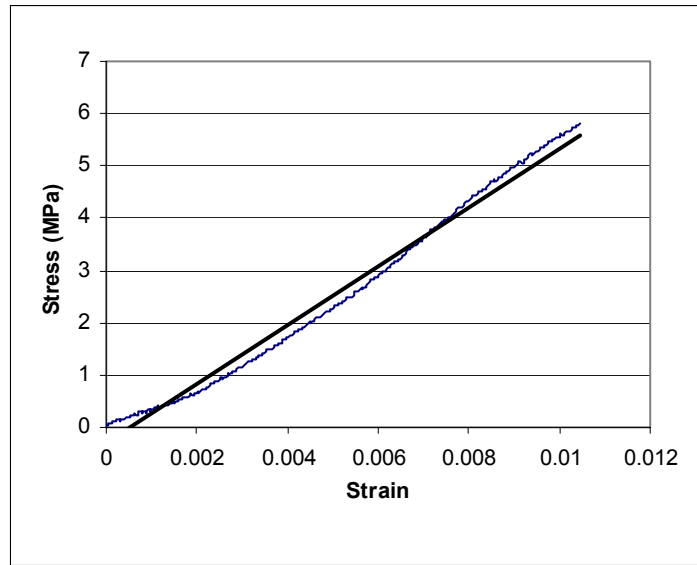


Figure 6 10 PPI with Elasto-plastic Fill Material (Expanded)

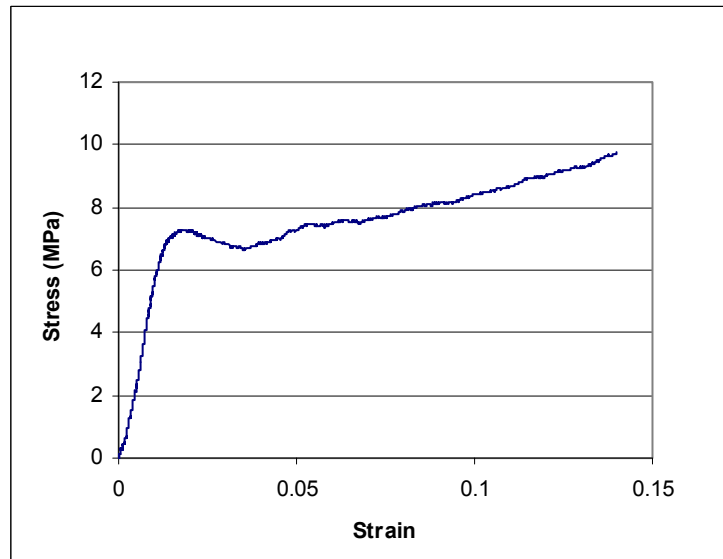


Figure 7 10 PPI with Elasto-Plastic Fill Material

THIS PAGE INTENTIONALLY LEFT BLANK

## **V. DISCUSSION AND RESULTS**

### **A. OPEN CELL ALUMINUM METAL FOAM**

The finite element model was compared against the analytic solutions presented by Gibson and Ashby [1] and experimental data of aluminum foam specimens compressed until failure occurred. The load on the cell in the FE model is applied on square cell face. From the results several observations may be made. When compressive load is applied the finite element model indicates nodal displacement in all axis. The undeformed model shows all faces are planar prior to application of compressive load. However, following application of a load the faces on which the load is not applied do not remain planar. The geometry of the tetrakaidecahedral results in a variable loading on edge elements, which is dependent upon the relative position of the element to the axis on which the load is applied. A non-uniform displacement of nodes will result due to the difference in axial and bending load present at any edge element. The intersections of the three edge elements at a vertex also act as a constraint upon the displacement and rotation of the edges. Figure 8 through Figure 10 show three different cell densities under compressive load. The un-deformed structure can be compared with the deformed state. The displacement of each node in the finite element model may be output for analysis as required.

The FE model was run to verify convergence and sensitivity to the change in the total number of elements per cell edge. Model convergence on a unique solution was based on relative change in displacement and moment depending on the number of elements selected. Table 4 is a representative summary of the maximum nodal displacement and moment for a given number of finite elements per edge. The data shows a maximum change in displacement of 0.25% when the number of elements is increased from one to three. When the number of elements is increased from 10 to 15 per edge the maximum change in displacement is approximately 0.081%. When 30 or more elements are used an oscillation is observed in the solution. This is likely due to reaching the machine precision of the computational model. These values confirm that the FE

model has reached a converged solution. The relative change in displacement and moment provided by increasing the number of finite elements to greater than fifteen may not justify the increased computing time required for the calculation. The data shows that a very good first approximation may be obtained from a single element solution.

No. of elements	x position	% Change	y position	% Change	moment	% Change
1	4.583		5.7991		1.2301	
3	4.5711	0.25965525	5.7933	0.100016	1.2317	0.129902
5	4.5593	0.25814355	5.7875	0.100116	1.2333	0.129733
10	4.5468	0.27416489	5.7814	0.1054	1.235	0.137652
15	4.5431	0.08137591	5.7796	0.031134	1.2355	0.040469
20	4.5416	0.0330171	5.7789	0.012112	1.2357	0.016185
25	4.5409	0.01541307	5.7785	0.006922	1.2358	0.008092
30	4.5404	0.01101103	5.7783	0.003461	1.2359	0.008091
35	4.5402	0.0044049	5.7782	0.001731	1.2359	0
40	4.54	0.00440509	5.7781	0.001731	1.236	0.008091
45	4.5399	0.00220264	5.7781	0	1.236	0

Table 4 Change in Maximum Displacement and Moment vs. Number of Finite Elements

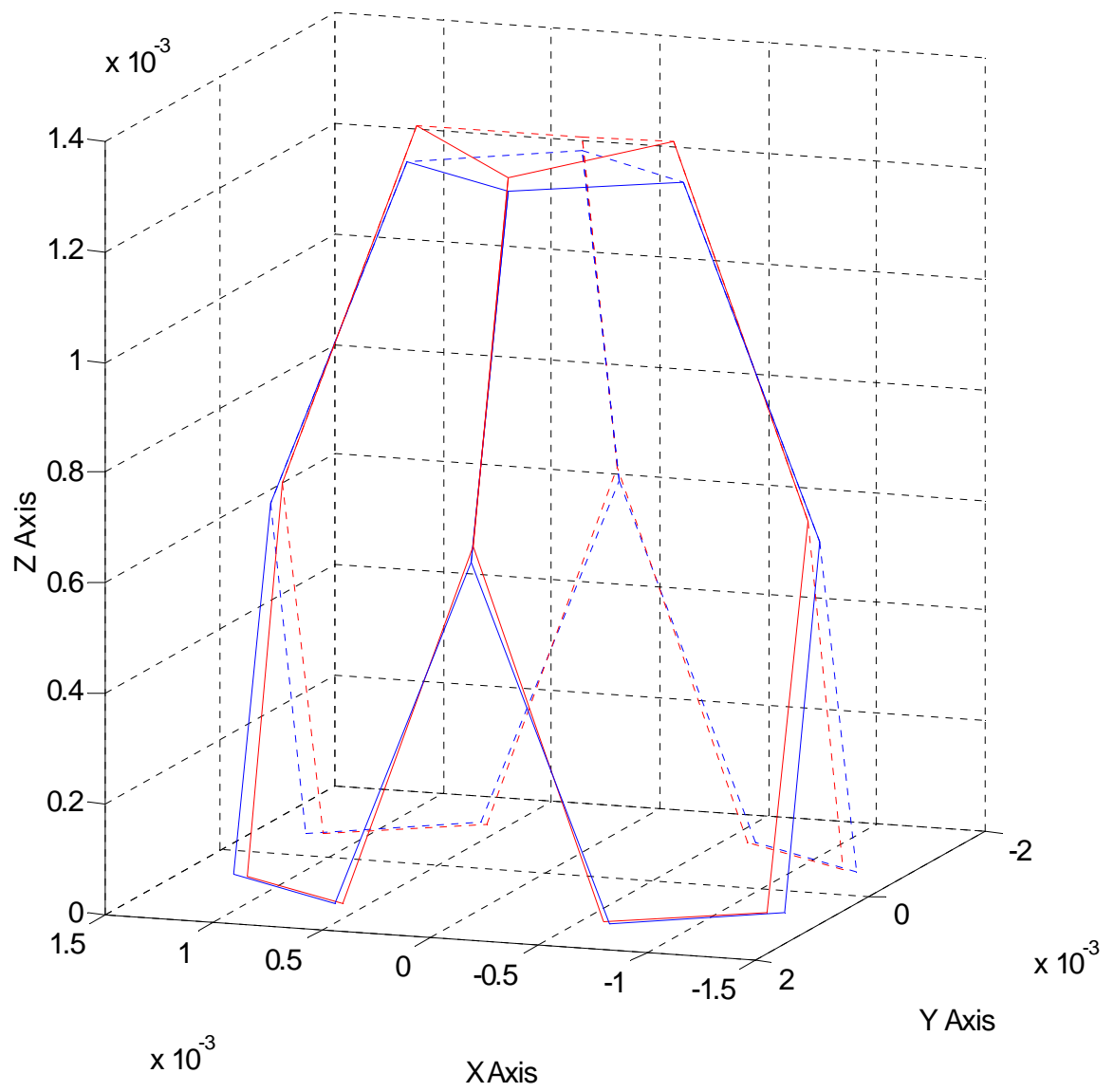


Figure 8 10 PPI Aluminum Compressed Cell

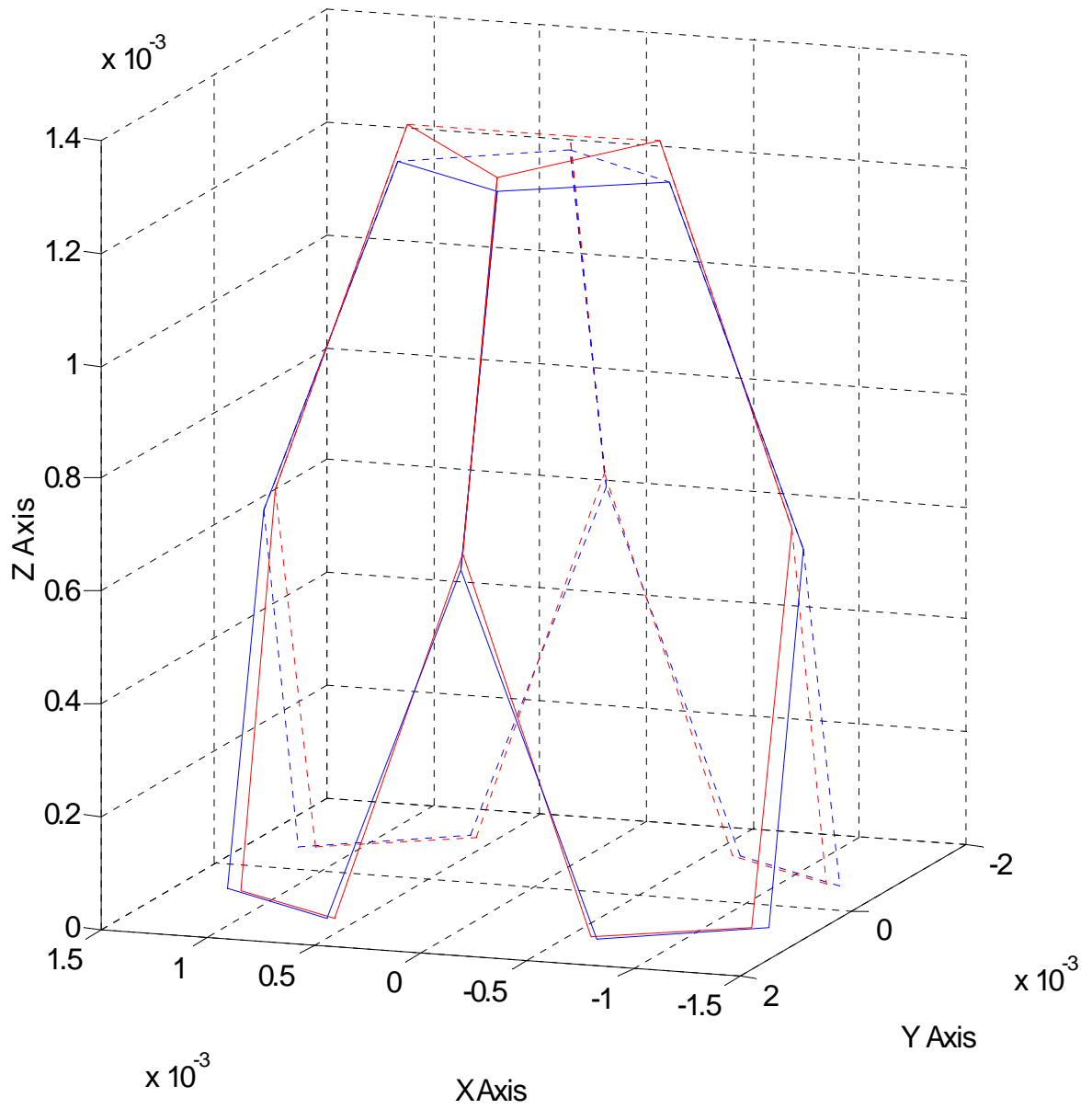


Figure 9 20 PPI Aluminum Compressed Cell

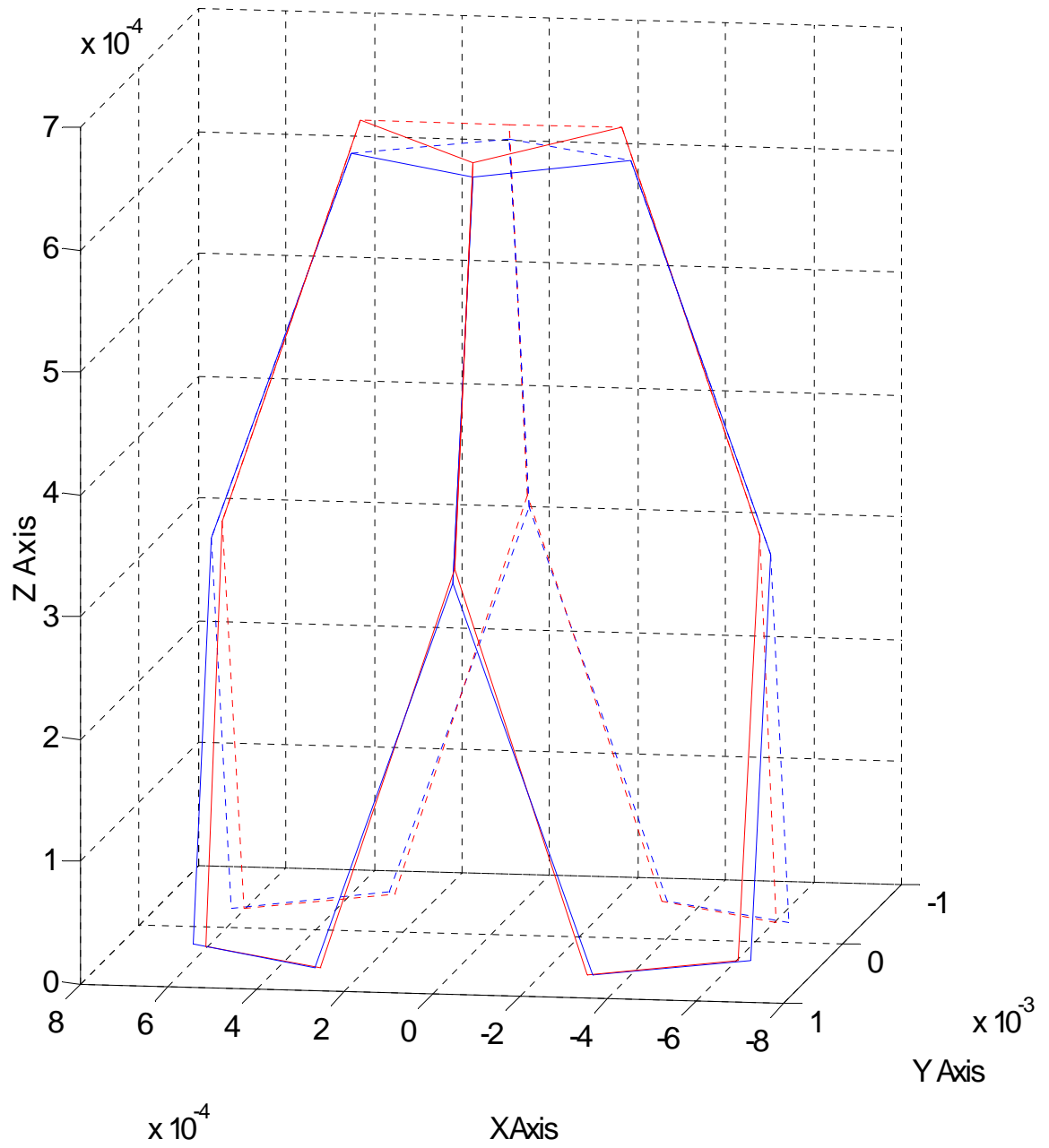


Figure 10 40 PPI Aluminum Compressed Cell



The finite element model shows good correlation with experimental analysis of stiffness for the range of density considered. Figure 11 shows stiffness as a function of relative density for the analytical, experimental and finite element model.

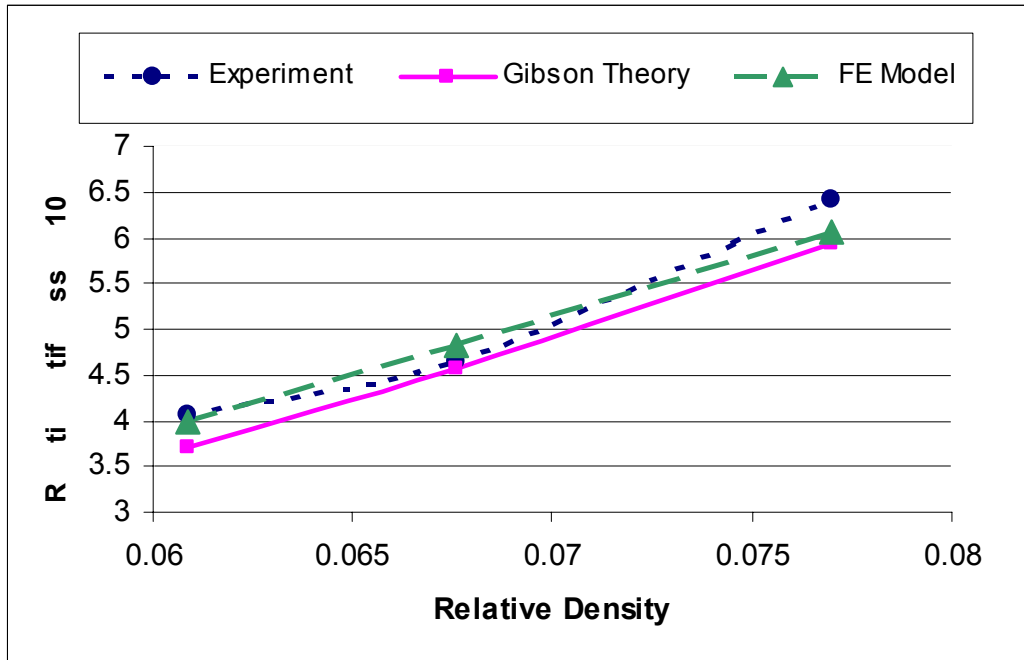


Figure 11 Relative Stiffness vs. Relative Density

The stiffness results correlate well amongst all methods. The data confirms the non-linear relation expected between density and stiffness. The analytical results were on average lower than the model prediction or those determined through experimentation. The experimental data shows a slightly higher order dependence on relative density than was observed with the analytical or finite element model. This result is potentially due to variation in experimental models and the non-uniform internal nature of real foam.

The strength of the foam is dependent upon the mechanism of failure. It was predicted that failure in the foam would occur due to plastic yielding at the edge elements because the slenderness ratio is relatively low for each foam edge. Figure 12 plots the relative strength versus relative density for the three analysis methods. The figure shows a very good correlation between experimental and FE methods. The empirical method of Gibson and Ashby was very conservative in predicting the plastic collapse strength.

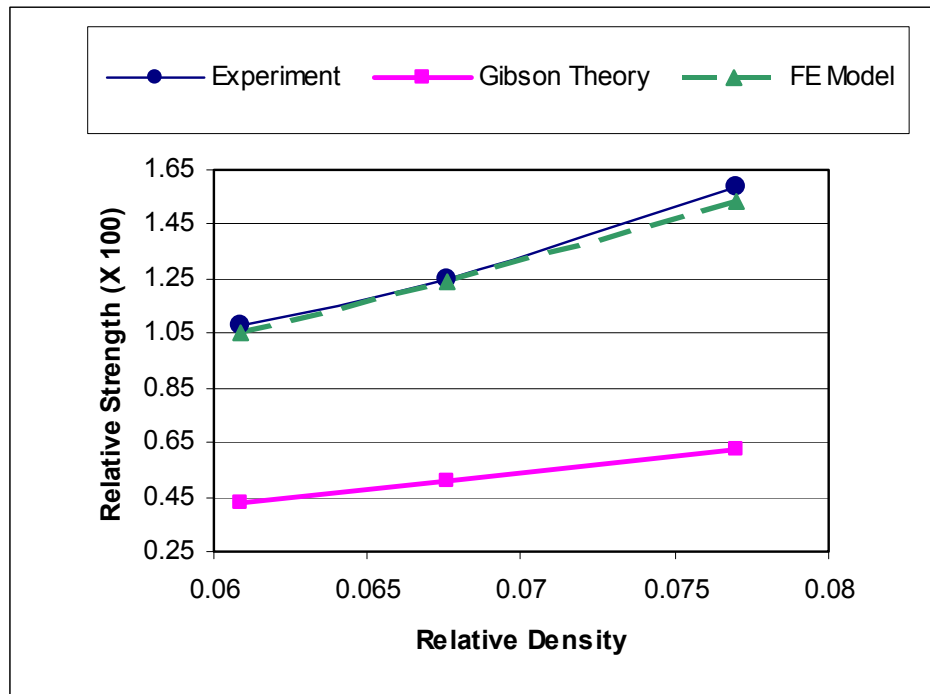


Figure 12 Relative Strength vs. Relative Density

The experiment results confirm a mild nonlinear relationship between relative density and strength. The experimental data shows some variability with results. This is potentially due to the non-uniform nature of real foam structures. The randomness of the real foam geometry does not appear to significantly impact the results.

Reviewing the displacement and moment results for each element shows that there are edge locations within the structure that may have locally higher stress concentrations, while the structure, as a whole has not undergone catastrophic failure. This is possibly due to the axial orientation of the edge in question relative to the direction of the load. When a Tetrakaidecahedral structure is loaded in compression on a face, the unit cell edges that are parallel to the face where the load is applied had smaller internal moments than other cell edges. This means that those edges provide less support to the structure under the compressive load. Even if the cell edges fail, the critical collapse may not occur as long as the remaining edges support the load. This shows that the strength of the unit cell is primarily provided by the cell edges that are not parallel to the loaded face. Failure of these cell edge elements will cause rapid degradation of overall cell integrity. This result was confirmed by experimentation and is consistent with results obtained by Park [21].

Collapse of the cell structure is controlled by failure of the edge elements, in either elastic buckling or exceeding the fully plastic moment. The location of failure is typically at the cell vertices. This is due to the unit cell behaving similar to a three dimensional frame structure. As previously noted, the large stiffness of the cell edges, coupled with their low mass, results in very high buckling stress values. The calculated fully plastic moment and corresponding plastic yield stress value is considerably lower. Therefore the mechanism of failure will likely be plastic collapse due to exceeding the fully plastic moment. The location of maximum moment for a clamped beam will occur at or near the ends. For the unit cell the joints/vertices of the cell represent the rigid or clamped beam end conditions. The clamped end condition is expected due to the discontinuity at the joints caused by a reorientation of the cell edge. If plastic collapse is the most probable method of failure, then significant deformation should be observable at these locations.

To confirm the mechanism of failure, scanning electron microscope (SEM) images were taken of representative sections of aluminum foam material before loading and just after plastic collapse. Appendix C has pre and post loading mages for various relative densities. Figure 13 shows the preloaded structure for 10 PPI foam. From these

images it is possible to see the unit cell and the orientation of the face in the foam matrix. This image confirms the selection of the tetrakaidecahedron as a good approximation for the basic geometry. The intersection of the edges and vertices are of interest. It is clear in the photo that mass is not uniformly distributed along the rod element. Some build up does occur at the vertices. However, this is relatively minor. The buildup of mass at the vertices will be more significant for calculating undamped natural frequency.

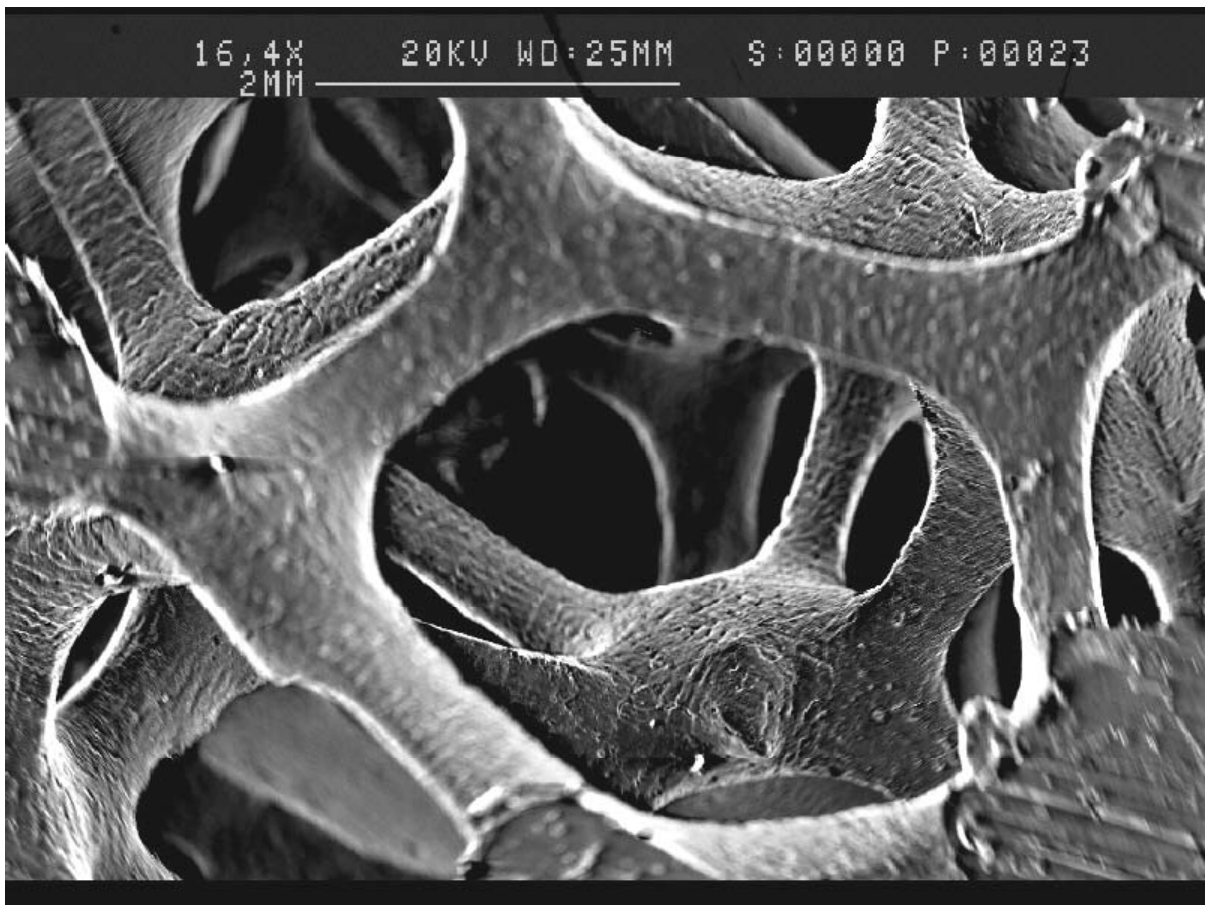


Figure 13 SEM Image of 10 PPI Aluminum Foam Before Compression

The post collapse image of Figure 14 clearly shows the plastic failure at the joints. This confirms the expectation that plastic failure will result in the aluminum cell. The image also shows the elongation of the cell following collapse.

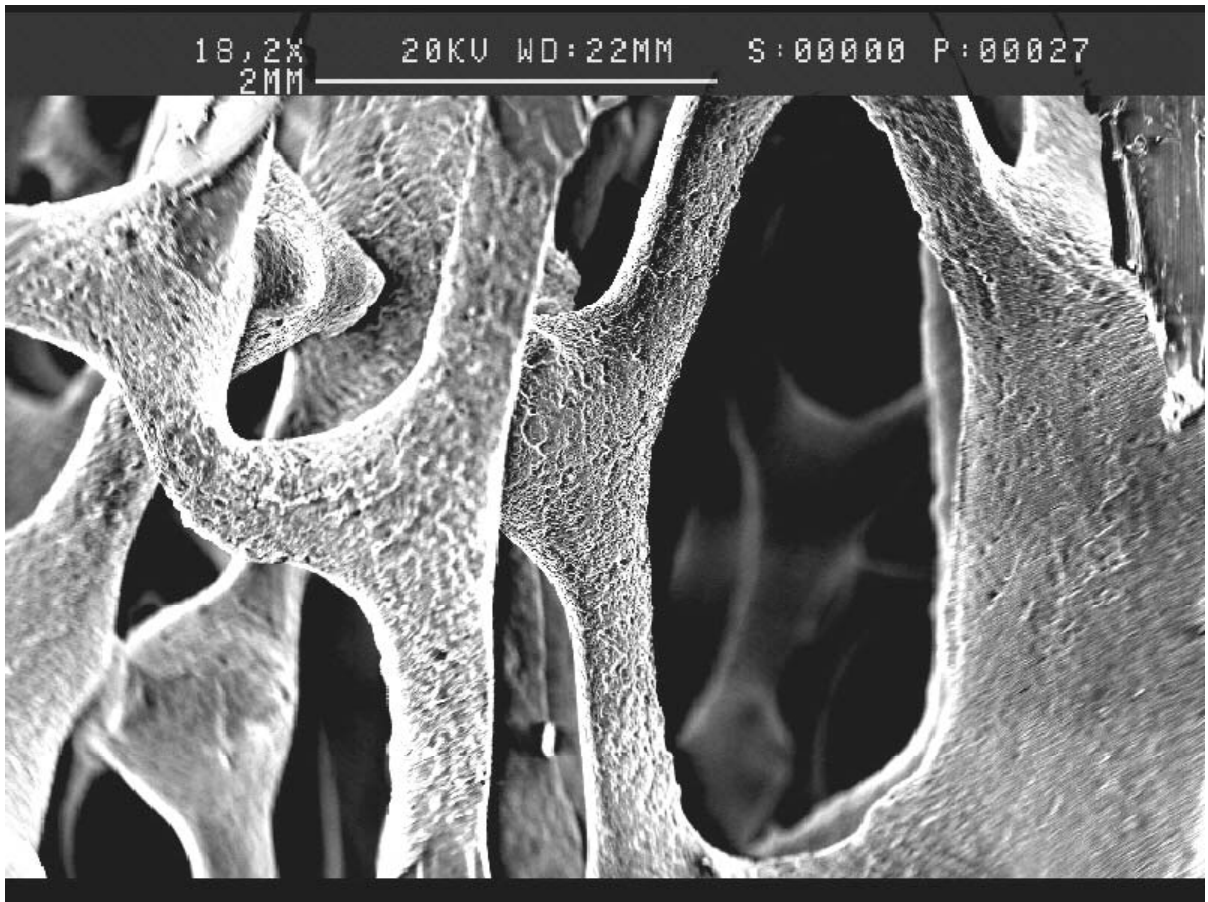


Figure 14 SEM Image of 10 PPI Aluminum Foam After Compression

The undamped natural frequency for the unit cell was compared to a frame rod structure clamped at both ends. This condition is chosen to represent the limitation on rotation and displacement associated with the vertices of the tetrakaidecahedra. The combination of a high stiffness, relatively short length and low mass of the rod elements results in a high predicted natural frequency. The FE model similarly predicted that the unit cell natural frequency would also be very high. The relatively high value for the first natural frequency of the unit cell implies that any structure created from metal foam will not be influenced by low frequency vibrations within the foam material but by whatever the lowest natural frequency possible, based on the geometry of the system. The high natural frequency of the structure also suggest that any low frequency forced vibrations on the structure will not excite the unit cell in a resonance mode. This fact is significant for naval acoustic applications that required reduced sympathetic vibrations. The lowest predicted natural frequency for three different densities of foam are summarized in the Table 5.

	10 PPI	20 PPI	40 PPI
FE Model (consistent mass method)	782 KHz	1.56 MHz	3.1 MHz
FE Model (lumped mass method)	1.5MHz	2.9MHz	5.7MHz
Beam Theory	774 KHz	1.4 MHz	2.9 MHz

Table 5 Beam Theory And Finite Element Model Predicted Natural Frequency

The finite element model results correlate well with beam theory. Further experimental investigation is required to correlate these results with real metal foam materials. Potential variations between model and real foams may be due to some simplification introduced by the model. One of the largest sources of error is the assumption that the mass is uniformly distributed about the rod. The SEM images clearly show that there is some lumping of mass at the vertices. This increased mass at the ends

of the rod will contribute to inertial effects of the mass about the axis of gyration for the rod. This increase in mass at the ends should have the impact of increasing the lowest natural frequency. This is consistent with results in Table 5 between the lumped mass method and the consistent mass method for determination of the cell natural frequency. The lowest natural frequency predicted by the lumped mass method was generally very close to the second frequency predicted by the consistent mass method.

A second source of error from this analysis method is the assumed uniform repeating nature of the cell structure within any real foam. Real metal foams have non-uniform cell structures. The randomness of real materials will result in cells with both shorter and longer elements, which will have different excitation frequencies. These random frequencies may or may not propagate throughout the foam due to the natural damping of the material. Although an analysis of damping within real foam was not completed, the non-uniform cell size within real foam would also contribute to any damping within the material. This result is expected due to increased mass at the vertex resulting in greater stiffness and less efficient transfer of energy between portions of the cell.

## B. FILLED ALUMINUM FOAM

The filled aluminum foam cell is expected to display similar properties to a closed cell tetrakaidecahedron. The problem with the closed cell empirical approach is that the fill material does not have the same material properties as the edge elements and therefore provides a varying degree of support to the edges depending on the stiffness of the filler. The stiffness of the fill material was significantly lower than the basic cell material therefore it will provide less support than a closed cell face of the same material. Additionally, the fill material will deform around the beam and potentially becomes displaced outside of the unit cell structure.

The finite element model shows good correlation with experimental analysis of stiffness for the range of density considered. Figure 15 shows relative stiffness as a function of relative density for experimental and finite element model. The model results were, on average, lower than those determined through experimentation.

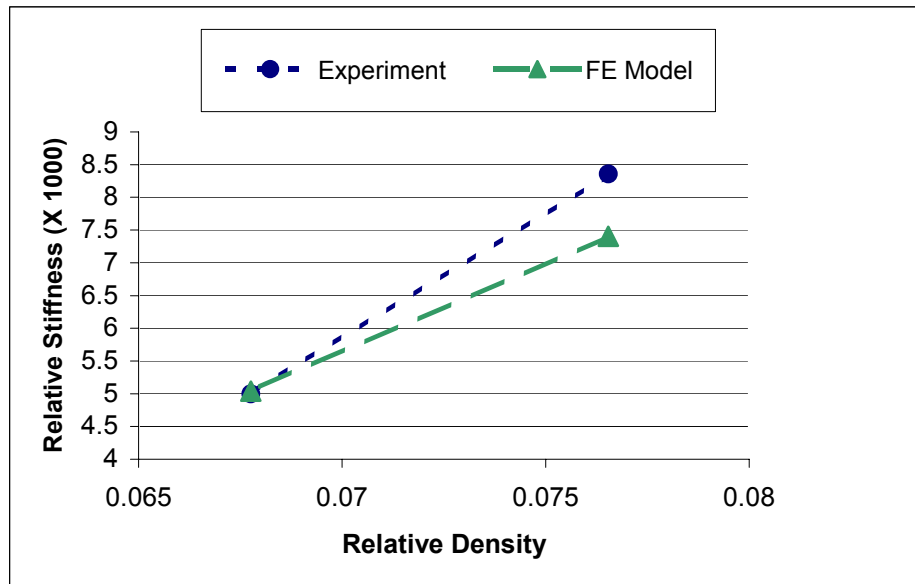


Figure 15 Filled Metal Foam Relative Stiffness vs. Relative Density



The strength of the foam is dependent upon the mechanism of failure. It was predicted that failure in the foam would occur due to plastic yielding at the edge elements because the slenderness ratio is relatively low for each foam edge. Figure 16 plots the relative strength versus relative density for the experimental and finite element methods. The figure shows a very good correlation between experimental and FE methods.

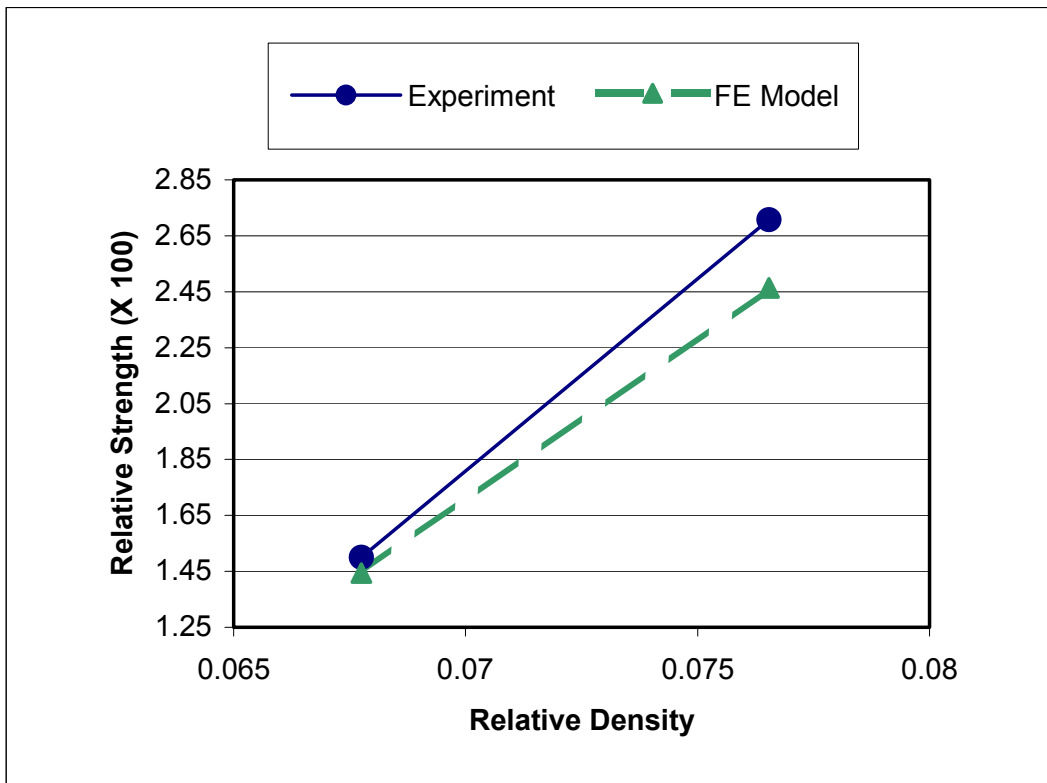


Figure 16 Filled Metal Foam Relative Strength vs. Relative Density

The model uses an elastic foundation to represent the support provided to each edge element and vertex. The density of the fill material and the sheer properties control the amount of bending within the edge elements. As expected, the unit cell filled with the elasto-plastic material will be stiffer. Hence we expected and obtained lower overall element displacements. This was confirmed by experimentation. Similarly, the model predicts a corresponding increase in the cell plastic strength. These results are summarized in Table 6 for two cases.

Strength (MPa)	10 PPI		40 PPI	
	Open Cell	Filled	Open Cell	Filled
Plastic	3.8	6.5	3.0	3.4

Table 6 Predicted Strength In Open Cell versus Filled Cell

For the filled case the added support of the viscoelastic material is assessed. The fill material will support the edge and vertices and will impact the axial displacement, bending and torsion of each of these structural elements. The model also assumes no friction between the unit cell and the fill material. It was found that the support of the fill in bending contributed most to the increased strength. Axial support effects were small however, their contribution becomes more pronounced as the sheer modulus of the material increases. Because we chose a uniform circular rod as our edge cross-section and because there is assumed on friction or restraint between the fill and the edge, torsion had the least impact on strength.

The model predicts that plastic collapse in the region of the hinges will govern the failure of the unit cell. This is due to the large moments at the hinge. The model predicts failure of the edge elements by plastic collapse with good correlation to experiments. There are several potential sources of error between the experimental and model predictions. The most common error is likely due to non-uniform cell size, shape and orientation. This error may have the effect of increasing or decreasing the apparent cell

stiffness. A second source of error is the incomplete fill of the metal foam with the viscoelastic material resulting in voids. Void formation will have the impact of decreasing the cell strength and making the filled cell appear more like the open cell. A third source of error is friction or connection between the fill material and the cell edges. This will result in a stiffer structure. In general, the observed strength was higher than the predicted. Table 7 summarizes this result.

Yield Strength (MPa)	10 PPI	40 PPI
FE Model Prediction	5.9	3.46
Experimental	6.5	3.6

Table 7 Predicted versus Observed Yield Strength

Figure 23 through Figure 26 in Appendix B show the stress strain diagrams for two representative filled aluminum foam elements.

## VI. CONCLUSION AND RECOMMENDATIONS

In this research the usefulness of the finite element method to predict the strength, stiffness and dynamic response of metal foam materials were investigated. The results from the model were in good correlation with experimental data. The significant findings of this research were:

- The use of the tetrakaidecahedron structure for analysis of metal foam materials provides reasonable solution accuracy without adding computational complexity required for more detailed geometries.
- The finite element model will accurately predict the failure strength of metal foam material with a better correlation to experimental results than will purely empirical approximations.
- The relatively high stiffness and low slenderness ratio for foam materials make it unlikely that collapse of cell edges will occur from Euler buckling. Empirical analysis and model results predicted that failure would occur by plastic collapse along cell edges. This was confirmed by scanning electron microscope images.
- The cell edges, which are parallel to the face where the load is applied, may fail without complete collapse of the tetrakaidecahedron structure. Plastic collapse or buckling in any edge that has an orientation not parallel to the face where the load is applied will lead to progressive collapse of the Kelvin ball.
- The predicted open cell model dynamic response was similar to that for a clamped beam structure. This result warrants further investigation.
- The high stiffness and low weight of the beam result in very high predicted undamped natural frequencies.
- When the metal foam is filled with visco-elastic material, the use of a beam on elastic foundation method is valid and provides results that are consistent with experiments and more accurate than a closed cell foam approximation.

This research investigated only a small range of relative densities for aluminum foam materials. Additional research using a wider selection of densities and with different material properties would help improve the model. Similarly, a wider selection of fill materials would help improve the accuracy of the model with respect to understanding the impact that the fill material has on cell stiffness

Additional experimentation is also required to validate the results of the dynamic model for open and closed cell foams. Testing with instrumented samples is necessary to confirm the frequency response of real structures. The real test data could be used to also determine the damping coefficient for foam material.

This research looked primarily at compressive loading along the face plane for a tetrakaidecahedron. The correlation of the model to experimental data should be done for both out of plane and pure shear load.

## APPENDIX A: STIFFNESS AND MASS MATRICES

Element Stiffness Matrix for the 3-D Frame Element

$$[K^e] = \begin{bmatrix} K_{11}^e & K_{12}^e \\ K_{21}^e & K_{22}^e \end{bmatrix}$$

$$[K_{11}] = \begin{bmatrix} a1 & 0 & 0 & 0 & 0 & 0 \\ 0 & b1 & 0 & 0 & 0 & b2 \\ 0 & 0 & c1 & 0 & -c2 & 0 \\ 0 & 0 & 0 & a2 & 0 & 0 \\ 0 & 0 & -c2 & 0 & 2*c3 & 0 \\ 0 & b2 & 0 & 0 & 0 & 2*b3 \end{bmatrix}$$

$$[K_{12}] = \begin{bmatrix} -a1 & 0 & 0 & 0 & 0 & 0 \\ 0 & -b1 & 0 & 0 & 0 & b2 \\ 0 & 0 & -c1 & 0 & -c2 & 0 \\ 0 & 0 & 0 & -a2 & 0 & 0 \\ 0 & 0 & c2 & 0 & c3 & 0 \\ 0 & -b2 & 0 & 0 & 0 & b3 \end{bmatrix}$$

$$[K_{21}] = \begin{bmatrix} -a1 & 0 & 0 & 0 & 0 & 0 \\ 0 & -b1 & 0 & 0 & 0 & b2 \\ 0 & 0 & -c1 & 0 & -c2 & 0 \\ 0 & 0 & 0 & -a2 & 0 & 0 \\ 0 & 0 & -c2 & 0 & c3 & 0 \\ 0 & b2 & 0 & 0 & 0 & b3 \end{bmatrix}$$

$$[K_{22}] = \begin{bmatrix} a1 & 0 & 0 & 0 & 0 & 0 \\ 0 & b1 & 0 & 0 & 0 & -b2 \\ 0 & 0 & c1 & 0 & c2 & 0 \\ 0 & 0 & 0 & a2 & 0 & 0 \\ 0 & 0 & c2 & 0 & 2*c3 & 0 \\ 0 & -b2 & 0 & 0 & 0 & 2*b3 \end{bmatrix}$$

where

$$a1 = EA/l; \quad a2 = G*J/l;$$

$$b1 = 12*E*I_z/(l^3); \quad b2 = 6*E*I_z/(l^2); \quad b3 = 2*E*I_z/(l);$$

$$c1 = 12*E*I_y/(l^3); \quad c2 = 6*E*I_y/(l^2); \quad c3 = 2*E*I_y/(l);$$

$E$  = Young's Modulus       $G$  = Shear Modulus       $A$  = cross-section area

$I_i$  = Moment of inertia in respective Axis (  $i = x, y$  or  $z$  )

$l$  = element length

## Elastic Foundation Stiffness Matrix

$$[K^e]_{foundation} = \begin{bmatrix} 2dc & 0 & 0 & 0 & 0 & 0 & dc & 0 & 0 & 0 & 0 & 0 \\ 0 & 156da & 0 & 0 & 0 & 22dal & 0 & 54da & 0 & 0 & 0 & -13dal \\ 0 & 0 & 156da & 0 & 22dal & 0 & 0 & 0 & 54da & 0 & -13dal & 0 \\ 0 & 0 & 0 & 2db & 0 & 0 & 0 & 0 & 0 & db & 0 & 0 \\ 0 & 0 & 22dal & 0 & 4dal^2 & 0 & 0 & 0 & 13dal & 0 & -3dal^2 & 0 \\ 0 & 22dal & 0 & 0 & 0 & 4dal^2 & 0 & 13dal & 0 & 0 & 0 & -3dal^2 \\ dc & 0 & 0 & 0 & 0 & 0 & 2dc & 0 & 0 & 0 & 0 & 0 \\ 0 & 54da & 0 & 0 & 0 & 13dal & 0 & 156da & 0 & 0 & 0 & -22dal \\ 0 & 0 & 54da & 0 & 13dal & 0 & 0 & 0 & 156da & 0 & -22dal & 0 \\ 0 & 0 & 0 & db & 0 & 0 & 0 & 0 & 0 & 2db & 0 & 0 \\ 0 & 0 & -13dal & 0 & -3dal^2 & 0 & 0 & 0 & 22dal & 0 & 4dal^2 & 0 \\ 0 & -13dal & 0 & 0 & 0 & -3dal^2 & 0 & 22dal & 0 & 0 & 0 & 4dal^2 \end{bmatrix}$$

where

$$da = kb \cdot l / 420; \quad db = kt \cdot l / 6; \quad dc = ka \cdot l / 6;$$

$$kt = kb \cdot r^{2/3}; \quad ka = G \cdot \text{ligament cross-section area};$$

$$k_b = \frac{8\pi G(1-\nu)}{(3-4\nu)K_0(2\pi r/\delta) + (\pi/\delta)K_1(2\pi r/\delta)}$$

$G$  = shear modulus of the filler       $\nu$  = Poisson's ration of the filler

$r$  = radius of the ligament       $\delta$  = ligament length

$K_0, K_1$  = zeroth order, first order modified Bessel function of the second kind

$l$  = element length



## Consistent Mass Matrix

$$[M^e]_{consistent} = mm * \begin{bmatrix} 140 & 0 & 0 & 0 & 0 & 0 & 70 & 0 & 0 & 0 & 0 & 0 \\ 0 & 156 & 0 & 0 & 0 & 22l & 0 & 54 & 0 & 0 & 0 & -13l \\ 0 & 0 & 156 & 0 & 22l & 0 & 0 & 0 & 54 & 0 & -13l & 0 \\ 0 & 0 & 0 & 2mb & 0 & 0 & 0 & 0 & 0 & mb & 0 & 0 \\ 0 & 0 & 22l & 0 & 4l^2 & 0 & 0 & 0 & 13l & 0 & -3l^2 & 0 \\ 0 & 22l & 0 & 0 & 0 & 4l^2 & 0 & 13l & 0 & 0 & 0 & -3l^2 \\ 70 & 0 & 0 & 0 & 0 & 0 & 140 & 0 & 0 & 0 & 0 & 0 \\ 0 & 54 & 0 & 0 & 0 & 13l & 0 & 156 & 0 & 0 & 0 & -22l \\ 0 & 0 & 54 & 0 & 13l & 0 & 0 & 0 & 156 & 0 & -22l & 0 \\ 0 & 0 & 0 & mb & 0 & 0 & 0 & 0 & 0 & 2mb & 0 & 0 \\ 0 & 0 & -13l & 0 & -3l^2 & 0 & 0 & 0 & 22l & 0 & 4l^2 & 0 \\ 0 & -13l & 0 & 0 & 0 & -3l^2 & 0 & 22l & 0 & 0 & 0 & 4l^2 \end{bmatrix}$$

where

$$mm = \frac{\rho \times A \times l}{420}$$

$\rho$  = ligament density

$l$  = element length

$A$  = cross-section area

$$mb = 35r^2$$

$r$  = radius of the ligament

## Lumped Mass Matrix

$$[M^e]_{lumped} = \frac{\rho \times area \times l}{6} \begin{bmatrix} 1 & 0 & 0 & 0 & 0 & 0 & 0 & 0 & 0 & 0 & 0 & 0 \\ 0 & 1 & 0 & 0 & 0 & 0 & 0 & 0 & 0 & 0 & 0 & 0 \\ 0 & 0 & 1 & 0 & 0 & 0 & 0 & 0 & 0 & 0 & 0 & 0 \\ 0 & 0 & 0 & 0 & 0 & 0 & 0 & 0 & 0 & 0 & 0 & 0 \\ 0 & 0 & 0 & 0 & 0 & 0 & 0 & 0 & 0 & 0 & 0 & 0 \\ 0 & 0 & 0 & 0 & 0 & 0 & 0 & 0 & 0 & 0 & 0 & 0 \\ 0 & 0 & 0 & 0 & 0 & 0 & 1 & 0 & 0 & 0 & 0 & 0 \\ 0 & 0 & 0 & 0 & 0 & 0 & 0 & 1 & 0 & 0 & 0 & 0 \\ 0 & 0 & 0 & 0 & 0 & 0 & 0 & 0 & 1 & 0 & 0 & 0 \\ 0 & 0 & 0 & 0 & 0 & 0 & 0 & 0 & 0 & 0 & 0 & 0 \\ 0 & 0 & 0 & 0 & 0 & 0 & 0 & 0 & 0 & 0 & 0 & 0 \\ 0 & 0 & 0 & 0 & 0 & 0 & 0 & 0 & 0 & 0 & 0 & 0 \end{bmatrix}$$

where

$\rho$  = ligament density

$l$  = element length

## Transformation Matrix

$$[T] = \begin{bmatrix} v_{11} & v_{21} & v_{31} & 0 & 0 & 0 & 0 & 0 & 0 & 0 & 0 & 0 \\ v_{12} & v_{22} & v_{32} & 0 & 0 & 0 & 0 & 0 & 0 & 0 & 0 & 0 \\ v_{13} & v_{23} & v_{33} & 0 & 0 & 0 & 0 & 0 & 0 & 0 & 0 & 0 \\ 0 & 0 & 0 & v_{11} & v_{21} & v_{31} & 0 & 0 & 0 & 0 & 0 & 0 \\ 0 & 0 & 0 & v_{12} & v_{22} & v_{32} & 0 & 0 & 0 & 0 & 0 & 0 \\ 0 & 0 & 0 & v_{13} & v_{23} & v_{33} & 0 & 0 & 0 & 0 & 0 & 0 \\ 0 & 0 & 0 & 0 & 0 & 0 & v_{11} & v_{21} & v_{31} & 0 & 0 & 0 \\ 0 & 0 & 0 & 0 & 0 & 0 & v_{12} & v_{22} & v_{32} & 0 & 0 & 0 \\ 0 & 0 & 0 & 0 & 0 & 0 & v_{13} & v_{23} & v_{33} & 0 & 0 & 0 \\ 0 & 0 & 0 & 0 & 0 & 0 & 0 & 0 & 0 & v_{11} & v_{21} & v_{31} \\ 0 & 0 & 0 & 0 & 0 & 0 & 0 & 0 & 0 & v_{12} & v_{22} & v_{32} \\ 0 & 0 & 0 & 0 & 0 & 0 & 0 & 0 & 0 & v_{13} & v_{23} & v_{33} \end{bmatrix}$$

where

$\bar{v}_1$  = a vector along the axis of the rod element;

$\bar{v}_2$  = a vector perpendicular to the rod element axis;

$\bar{v}_3$  = a vector perpendicular to  $\bar{v}_1$  and  $\bar{v}_2$ ;

$\bar{v}_a$  = a vector pointing to the origin  $[0 \ 0 \ 0]$  of the global axis from the starting point of the  $\bar{V}_1$  vector;

$$\bar{v}_2 = \bar{v}_1 \times \bar{v}_a$$

$$\bar{v}_3 = \bar{v}_1 \times \bar{v}_2$$

## APPENDIX B: STRESS-STRAIN DIAGRAMS

### 1. 10 PPI

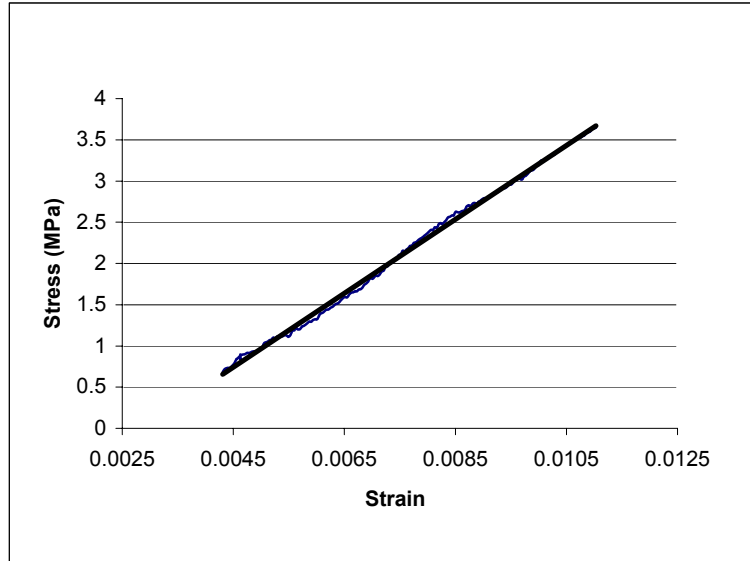


Figure 17 10 PPI Stress vs. Strain (Expanded)

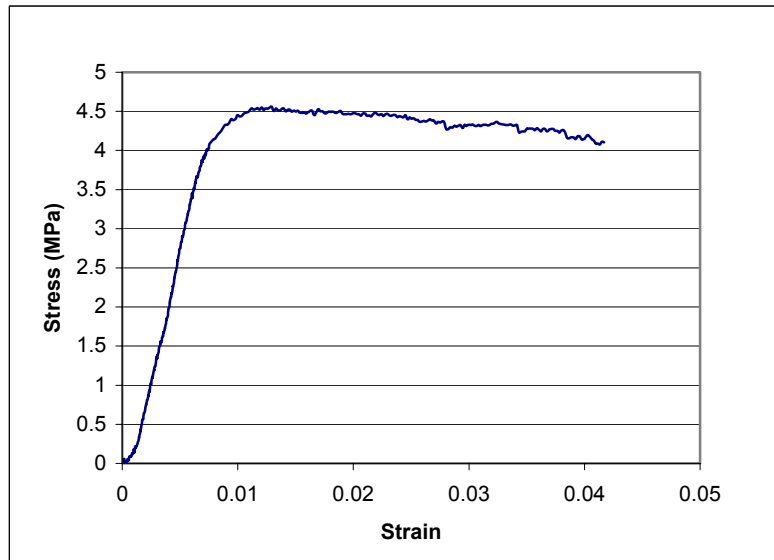


Figure 18 10 PPI Stress vs. Strain

## 2. 20 PPI

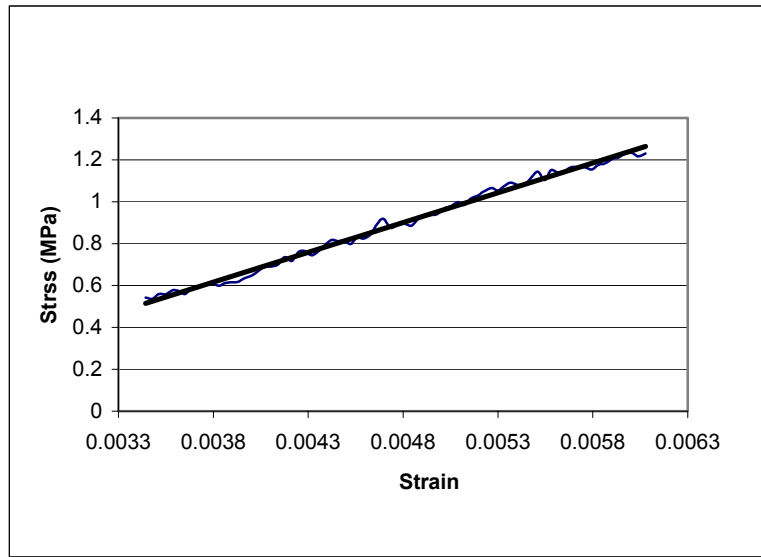


Figure 19 20 PPI Stress vs. Strain (Expanded)

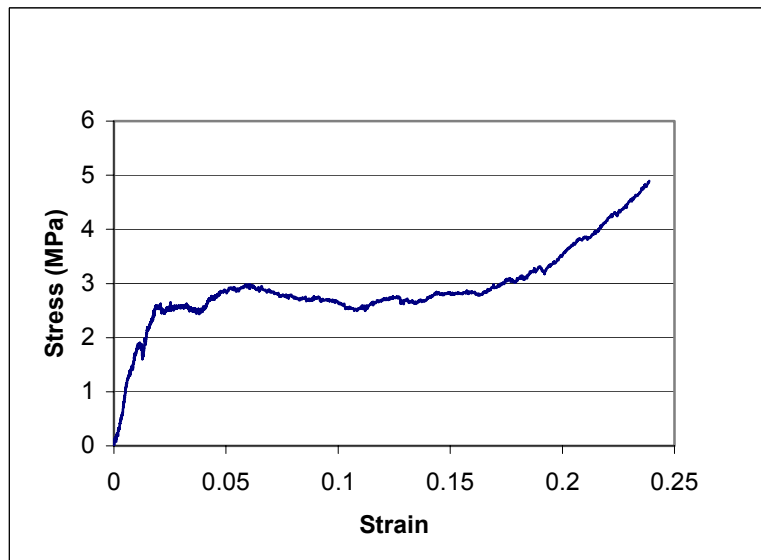


Figure 20 20 PPI Stress vs. Strain

### 3. 40 PPI

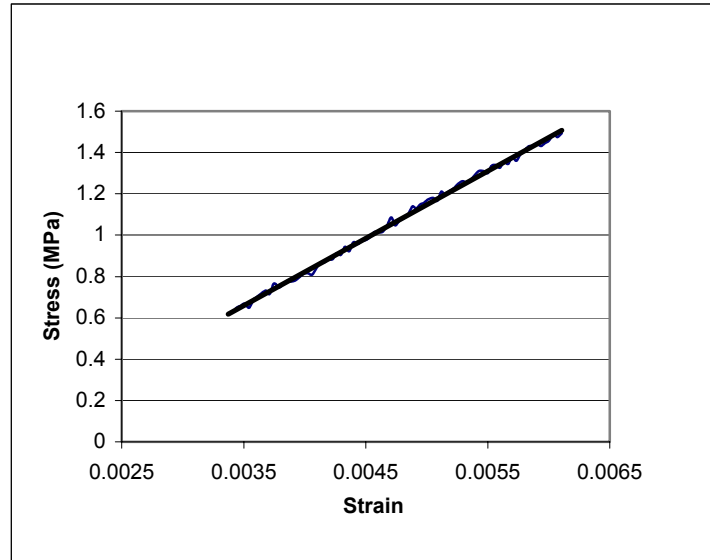


Figure 21 40 PPI Stress vs. Strain (Expanded)

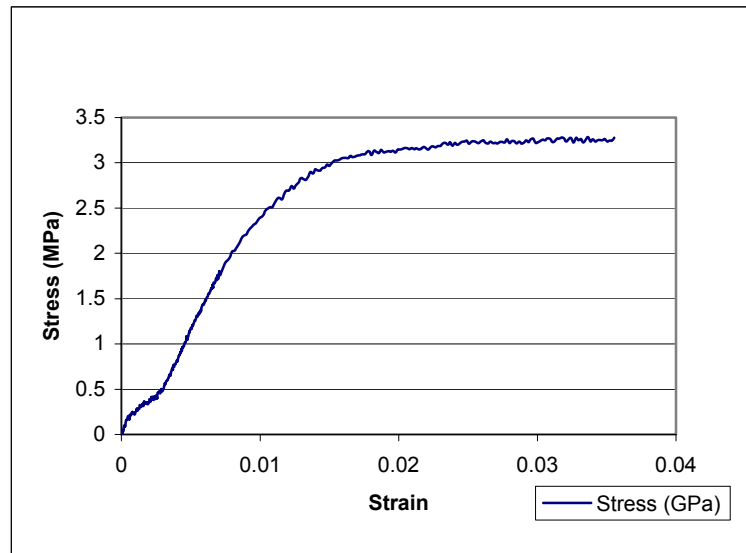


Figure 22 40 PPI Stress vs. Strain

#### 4. 10 PPI + FILL MATERIAL

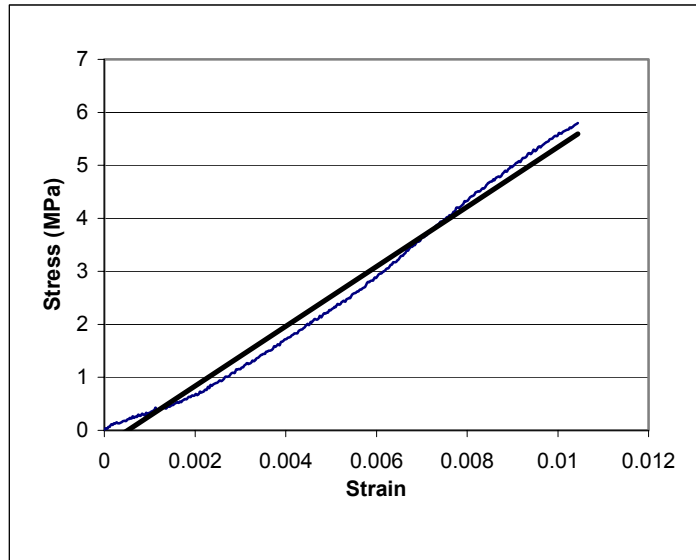


Figure 23 10 PPI + Fill Stress vs. Strain (Expanded)

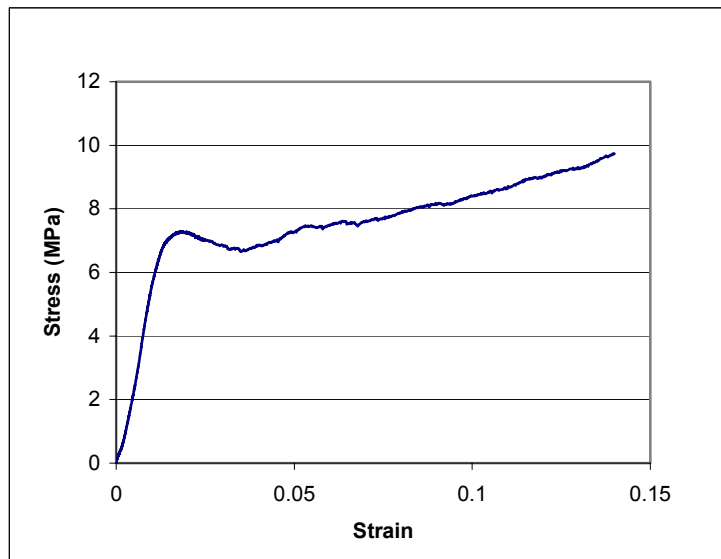


Figure 24 10 PPI + Fill Stress vs. Strain

## 5. 40 PPI + FILL MATERIAL

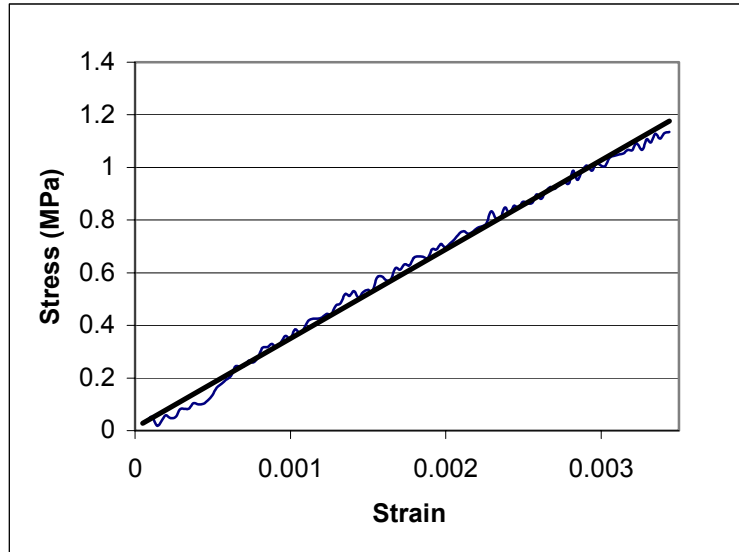


Figure 25 40 PPI + Fill Stress vs. Strain (Expanded)

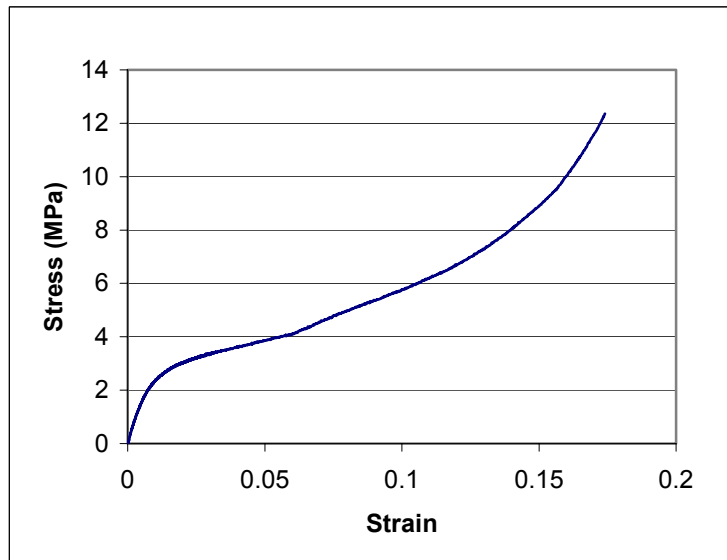


Figure 26 40 PPI + Fill Stress vs. Strain



THIS PAGE INTENTIONALLY LEFT BLANK

## APPENDIX C: SCANNING ELECTRON MICROSCOPE IMAGES

### 1. 10 PPI IMAGES



Figure 27 SEM Image of 10 PPI Aluminum Foam Before Compression

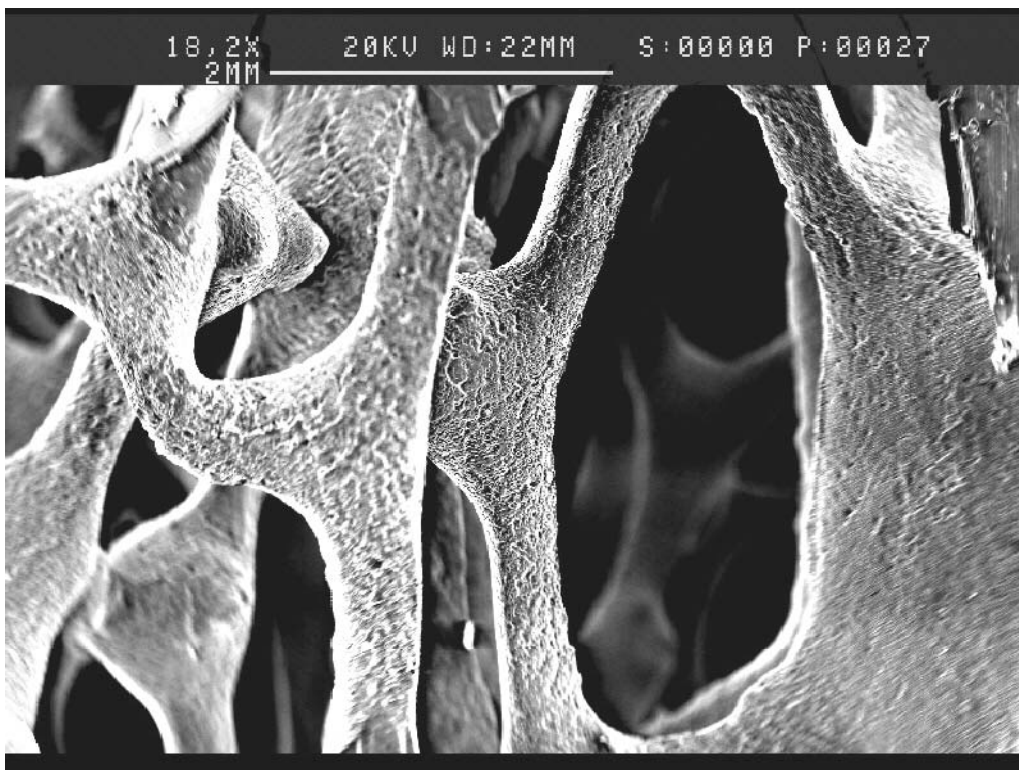


Figure 28 SEM Image of 10 PPI Aluminum Foam After Compression

## 2. 20 PPI IMAGES

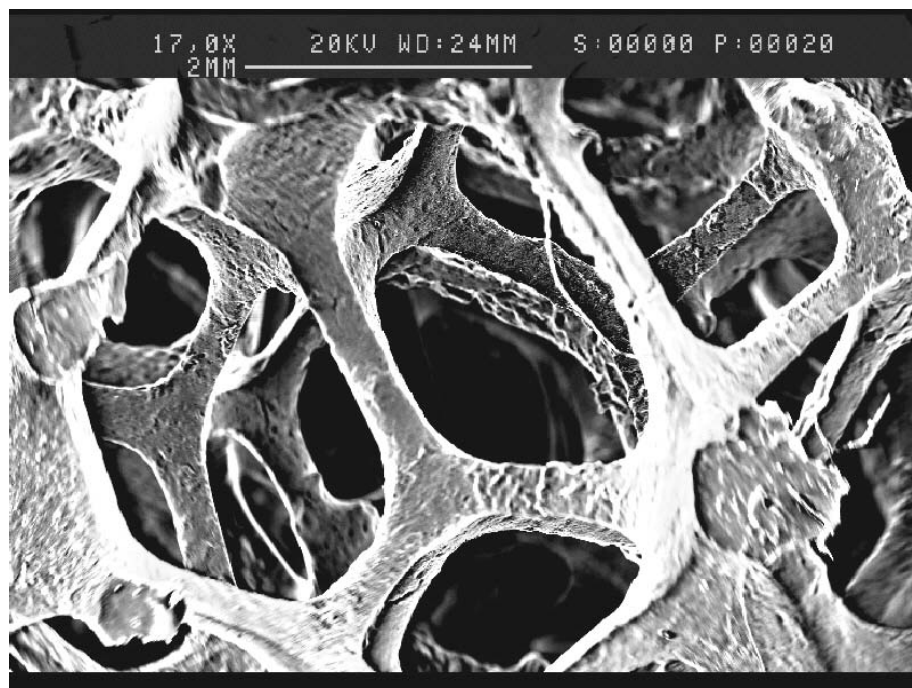
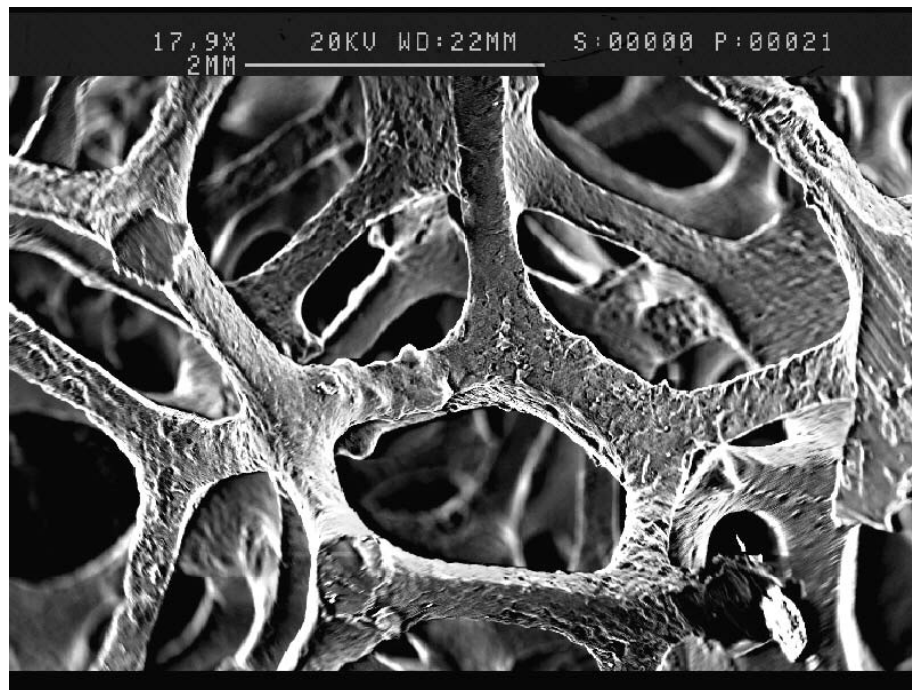


Figure 29 SEM Image of 20 PPI Aluminum Foam Before Compression

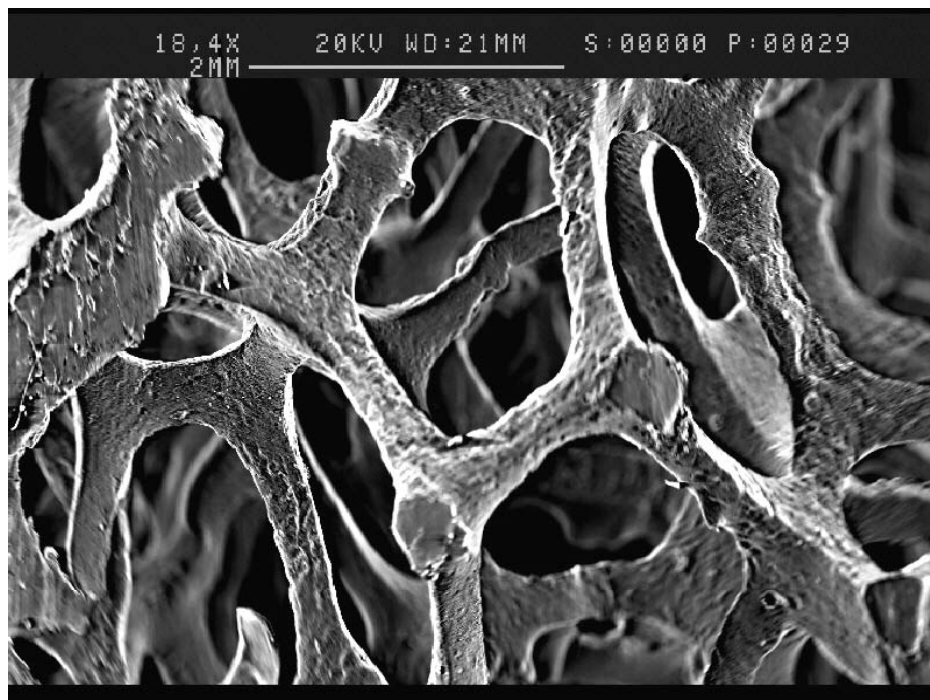
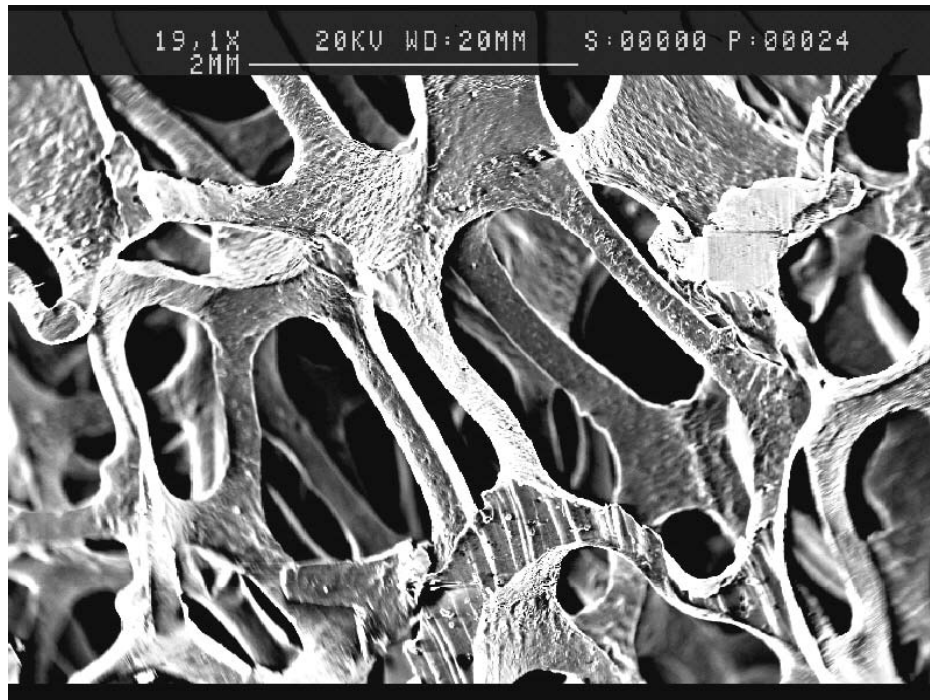


Figure 30 SEM Image of 20 PPI Aluminum Foam After Compression

### 3. 40 PPI IMAGE

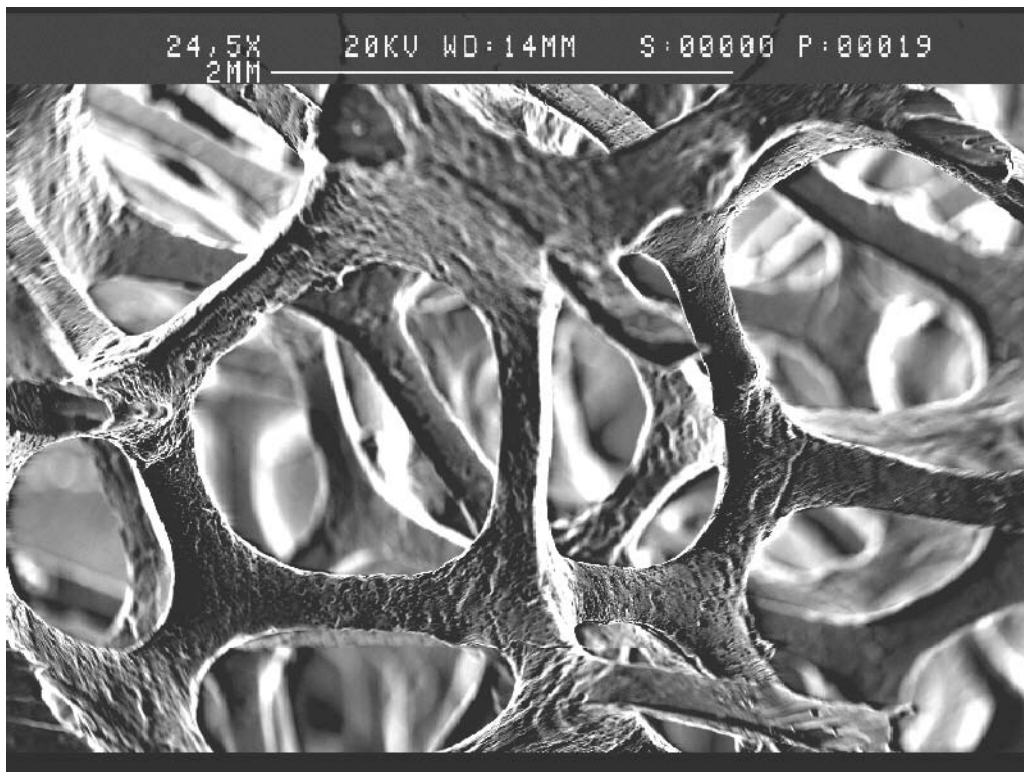


Figure 31 SEM Image of 40 PPI Aluminum Foam Before Compression

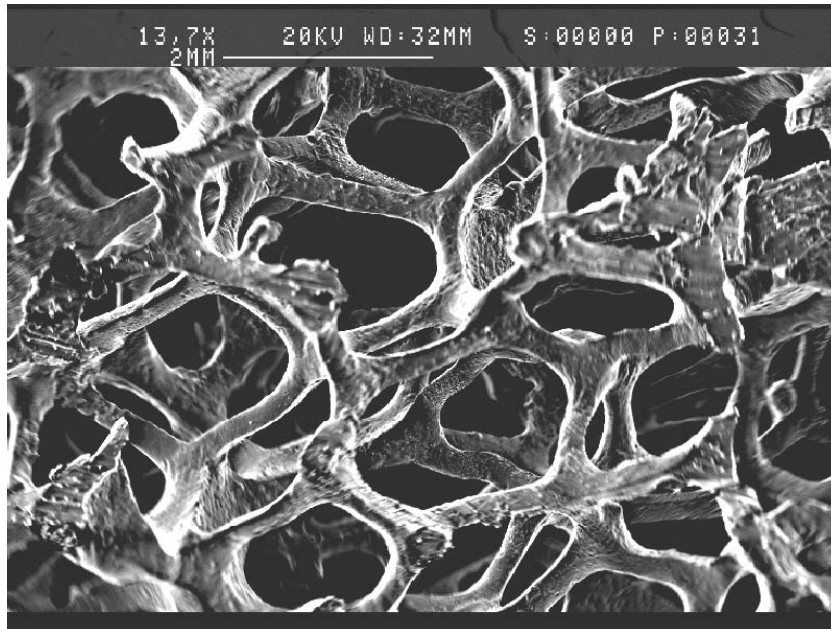
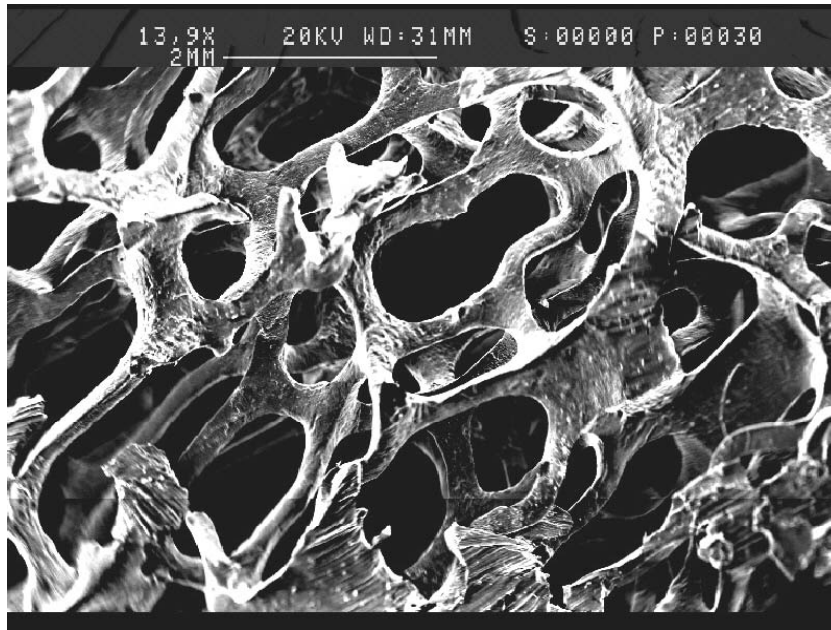


Figure 32 SEM Image of 40 PPI Aluminum Foam After Compression



## LIST OF REFERENCES

- [1] Gibson, Lorna J., Ashby, Michael F., (1997) *Cellular Solids: Structures and Properties*, 2<sup>nd</sup> ed, Cambridge University Press, Cambridge.
- [2] Kelvin, Lord(Sir W. Thompson) (1887) *Phil. Mag.*, 24, 503.
- [3] Noor, A.K., (1988) Continuum Models for Repetitive Lattice Structures, *Applied Mechanics Review*, 7, July.
- [4] Kogbetliantz, E. G., (1969) *Fundamentals of Mathematics from an Advanced Viewpoint*, Gordon and Breach Science Publishers, New York.
- [5] War Department, (1944) *Solid Geometry*, Ginn and Company, Washington, DC.
- [6] Noor, A.K., Anderson, M.S., Greene, W. H., “Continuum Models for beam and Platelike Lattice Structures,” *AIAA Journal*, 16,12.
- [7] Garboczi, E. J. & Roberts, A. P., (2000) Elastic Properties of Model Random Three-Dimensional Open Cell Solids [Online Report]. Available URL: <http://ciks.cbt.nist.gov/~garbocz/opencell/oc02a.html>
- [8] Platonic Solids, 1997-2001, Platonic Realms [Online report]. Available URL: <http://www.mathacademy.com/pr/prime/articles/platsol/index.asp>
- [9] Hart, George W., 1996, Archimedean Semi-Regular Polyhedra, [Online Report]. Available URL: <http://www.georgehart.com/virtual-polyhedra/archimedean-info.html>
- [10] Zhu, H. X., Knott J. F., and Mills, N. J., (1997) “Analysis of the elastic properties of open-cell foams with tetrakaidecahedral cells,” *J. Mech. Phys. Solids*, 45,319-343.
- [11] Weaire, D and Phelan, R., (1994) A counter-example to Kelvin’s conjecture on minimal surfaces, *Phil. Mag. Lett.* 69,107-10.
- [12] TCD Foam Physics Group, Weaire-Phelan Structure [Online report]. Available URL: <http://www.maths.tcd.ie/~shahs/index2.html>
- [13] Hodge, PHILIP G., *Plastics Analysis of Structures*, McGraw-Hill, New York, 1959.
- [14] Ko, W.L. , (1965) *J. Cell. Plast.* 1, 45-50.



- [15] Mills, N. J. (2000) "Micromechanics of Polymeric foams," *2000 Nordic meeting on Materials and Mechanics*, 3<sup>rd</sup>, 45-76.
- [16] Ugural, Ansel C., Fenster Saul K., *Advances Strength and Applied Elasticity*, 3<sup>rd</sup>, Prentice Hall PTR, Upper Saddle River, 1995.
- [17] Kwon, Young W. & Bang, Hyochong, (2000) *The Finite Element Method: Using MATLAB*, 2<sup>nd</sup>, CRC Press, Boca Raton.
- [18] Nuebert, V. H., (1971) Relationship of Substructuring to Improvement of Dynamic Modeling, Pennsylvania State University.
- [19] Dow, J.O., Huyer, S.A., (1984) "Continuum Models of Space Station Structures," *Journal of Aerospace Engineering*, December.
- [20] Grendstedt, J. L., (1998) *J. Mech. Phys. Solids*, 46, 29-50.
- [21] Park, Chanman (2000) *Development of Steel Foam Processing Methods and Characterization of Metal Foam*, Ph.D. Dissertation, University of Southern California, Los Angeles, California.

## INITIAL DISTRIBUTION LIST

1. Defense Technical Information Center  
Ft. Belvoir, Virginia
2. Dudley Knox Library  
Naval Postgraduate School  
Monterey, California
3. Engineering & Technology Curricular Office (Code34)  
Naval Postgraduate School  
Monterey, California
4. Professor Young Kwon  
Naval Postgraduate School  
Monterey, California
5. Professor Young Shin  
Naval Postgraduate School  
Monterey, California
6. Dr. Chanman Park  
Naval Postgraduate School  
Monterey, California
7. LCDR Rabon Cooke, USN  
3453 Ingraham Street, #417  
San Diego, California

